

Machine Learning Aided Fracture Surface Analysis of Additively Manufactured Lattice  
Structures Subjected to Uniaxial Tensile Loading

by

Francis Maxwell Sampson

Department of Mechanical Engineering and Materials Science  
Duke University

Defense Date: November 20, 2024

Approved:

Kenneth Gall – Thesis Advisor

Lynda Catherine Brinson

George Delagrammatikas

Thesis submitted in partial fulfillment of the requirements for the degree of Master of  
Science in the Department of Mechanical Engineering and Materials Science in The Graduate  
School of Duke University  
2024

ABSTRACT

Machine Learning Aided Fracture Surface Analysis of Additively Manufactured Lattice Structures Subjected to Uniaxial Tensile Loading

by

Francis Maxwell Sampson

Department of Mechanical Engineering and Materials Science  
Duke University

Defense Date: November 20, 2024

Approved:

Kenneth Gall – Thesis Advisor

Lynda Catherine Brinson

George Delagrammatikas

An abstract of a thesis submitted in partial fulfillment of the requirements for the degree of Master of Science in the Department of Mechanical Engineering and Materials Science in The Graduate School of Duke University  
2024

Copyright by  
Francis Maxwell Sampson  
2024

## **Abstract**

Additive manufacturing (AM) is a continuously developing and growing manufacturing process that provides a means for more efficient and rapid production of 3D parts. A major application of AM includes production of lattice structures which are highly complex, periodic parts that are difficult to fabricate with conventional manufacturing methods. These lattice structures can be used in a multitude of industries because of their desirable mechanical properties and high strength-to-weight ratio and are particularly attractive for load-bearing biomedical implants for bone regeneration. The need for these structures as implants requires an understanding of their mechanical properties as well as their fracture behavior in the event of unexpected failure. This study examined and characterized the mechanical properties and fracture mechanics of cylindrical AM lattice structures subjected to uniaxial tension. These lattice structures were designed using two different unit cells, four porosity values, ten materials and six printing technologies. The structures were imaged using micro-computed tomography (micro-CT) and scanning electron microscopy (SEM) to observe the fracture surfaces. These fracture surfaces were then converted as inputs for predictive machine learning models that worked to determine the fourth order plane of best fit to the broken lattice structure. The results of the study showed that lattice structures fabricated using Multi Material Jetting (MMJ) had the best mechanical performance in terms of normalized lattice strength and normalized strain at break. Gyroid structures had superior mechanical properties to the octet unit cell structures. It was also observed that a power function can describe the relationship between material ultimate strength and mechanical ultimate strength. The machine learning models used were Kernel Ridge Regression, Polynomial Regression, and Random Forest, with the Random Forest demonstrating the lowest root mean squared error for test data at a value of 0.333.

## **Dedication**

This thesis is dedicated to my grandfather and namesake, Francis Maxwell Abboa-Opare, and my cousin Emmanuel Opare. I love you both, rest easy.

Far in distance, but always close in love and spirit.

Ghana to the world.

# Contents

Abstract.....	iv
List of Tables .....	x
List of Figures.....	xi
Acknowledgements.....	xii
1. Introduction.....	1
1.1 Objective .....	4
1.2 Thesis Outline.....	5
2. Additive Manufacturing Technologies .....	6
2.1 Introduction .....	6
2.1.1 Process.....	6
2.2 Material Extrusion.....	7
2.2.1 Fused Deposition Modeling .....	8
2.3 Vat Photopolymerization.....	8
2.3.1 Digital Light Processing.....	9
2.4 Jetting Technology .....	9
2.4.1 Multi Material Jetting.....	10
2.5 Laser Powder Bed Fusion.....	10
2.5.1 Multi Jet Fusion.....	10
2.5.2 Selective Laser Sintering.....	11
2.5.3 Selective Laser Melting.....	11
2.6 Chapter Summary.....	12
3. Additively Manufactured Lattice Structures.....	13
3.1 Introduction .....	13
3.2 Applications.....	13

3.2.1 Biomedical Implants for Bone Regeneration .....	14
3.2.2 Geometry .....	15
3.3 Unit Cells.....	15
3.3.1 Strut-Based Unit Cells.....	16
3.3.2 Sheet-Based Unit Cells.....	17
3.4 Chapter Summary .....	17
4. Materials and Methods.....	18
4.1 Introduction .....	18
4.2 Lattice Structure Design.....	18
4.2.1 Unit Cells.....	18
4.2.2 Porosity.....	19
4.3 Fabrication of Cylindrical Lattice Structures .....	19
4.3.1 Fused Deposition Modeling .....	20
4.3.2 Digital Light Processing .....	21
4.3.3 Multi Material Jetting.....	21
4.3.4 Multi Jet Fusion.....	21
4.3.5 Selective Laser Sintering.....	21
4.3.6 Selective Laser Melting.....	22
4.4 Porosity Validation.....	24
4.5 Mechanical Characterization .....	25
4.6 Microstructural Imaging for Fracture Analysis .....	26
4.6.1 Scanning Electron Microscopy .....	26
4.6.2 Micro Computed Tomography.....	27
4.7 Chapter Summary .....	29
5. Machine Learning Model and Theory .....	30

5.1 Introduction .....	30
5.2 Code Breakdown .....	30
5.2.1 Preprocessing and Initialization .....	30
5.2.2 Defining Fracture Surfaces and Plane Fitting .....	31
5.3 Machine Learning Setup .....	32
5.3.1 Inputs and Outputs .....	32
5.3.2 Principal Components Analysis for Feature Reduction .....	32
5.4 Model Architecture for Algorithms Used.....	33
5.4.1 Kernel Ridge Regression.....	33
5.4.2 Polynomial Regression.....	34
5.4.3 Random Forest .....	34
5.5 Evaluating Model Performance.....	35
5.5.1 Metrics.....	35
5.5.2 Feature Importance.....	36
5.4 Chapter Summary.....	36
6. Results.....	37
6.1 Porosity.....	37
6.2 Mechanical Testing .....	39
6.3 Imaging.....	40
6.4 Machine Learning.....	43
6.5 Chapter Summary.....	43
7. Conclusions.....	44
7.1 Discussion .....	44
7.1.1 Porosity.....	44
7.1.2 Mechanical Performance.....	45

7.1.3 Fracture Mechanics .....	46
7.1.4 Machine Learning .....	47
7.2 Future Work .....	48
References.....	50

## List of Tables

Table 1: Material Properties.....	24
Table 2: Machine Learning Model Performance. ....	43

## List of Figures

Figure 1: Strut-Based Unit Cells.....	16
Figure 2: Sheet-Based Unit Cells.....	17
Figure 3: CAD Renderings and Printed Samples for 50% Porosity Lattices and Solid Structures. .....	23
Figure 4: Weight-Based Porosity Validation Process.....	24
Figure 5: Mechanical Testing Setup. ....	25
Figure 6: Micro-CT Setup for Batch Scanning of Fractured AM Lattice Structures.....	28
Figure 7: Process for Defining Fracture Surfaces and 4 <sup>th</sup> Order Plane of Best Fit. ....	31
Figure 8: Explained Variance vs Number of Components. ....	33
Figure 9: Machine Learning Flowchart. ....	35
Figure 10: CT Data Displaying Porosity Values for Octet Lattice Structures and Printing Discrepancies Affecting Porosity. ....	37
Figure 11: Designed Porosity vs. Experimental Porosity. ....	38
Figure 12: Normalized Lattice Ultimate Strength.....	39
Figure 13: Material Ultimate Strength vs. Normalized Ultimate Strength. ....	40
Figure 14: CT Data Showing 50% Porosity Lattice Structures Before and After the Onset of Fracture. ....	41
Figure 15: SEM Images of 70% Porosity Lattice Structures Using Different Detectors.....	42

## Acknowledgements

All honor and glory belong to the God I serve.

I would like to acknowledge the contributions of the Duke University Department of Mechanical Engineering and Materials Science (MEMS), the Graduate School, the Shared Materials Instrumentation Facility (SMiF), and the GEM Fellowship for making it possible to pursue a graduate degree and find work that was meaningful and impactful to me. The work presented in this thesis is not possible without this collaboration. I am thankful to my thesis committee members—Ken Gall, Cate Brinson, and George Delagrammatikas—for the support and cooperation during the development of this work. An extra thanks goes to George Delagrammatikas in his role as my Director of Master’s Studies in the MEMS cohort as well. With all your responsibilities, you managed to keep my best interests at heart, and you actively ensured my success even before I officially enrolled at this university. I am forever grateful for your commitment to me.

I would like to personally thank those in the Gall Group at Duke University. Thank you to my advisor, Ken Gall, for your help with the execution of this project and for your feedback. Though our interactions early into my time at Duke were limited, I am excited to see the ways in which this work can impact research in additive manufacturing. To Jake Peloquin, Niusha Daneshdoost, and Caroline Alting—thank you for the guidance, the collaboration, and the overwhelming friendship for the duration of my time in the lab. You have all supported me and encouraged me in so many ways, and I am forever indebted to you all for making my experience a great one. Special thanks to Jake, for being a mentor, teacher, and friend all in one by ensuring that my integration and understanding in the lab was valuable and of equal importance to the research being conducted.

Finally, I would like to thank my family and friends. To my parents, James and Felicia, and my older siblings, Lisa and Jonathan—thank you for being my safe space. Your love and constant words of affirmation, all my life but especially during my studies, were always delivered at the right moments. To know that I was loved and made you all proud continually reminded me that the sacrifices that we have made have not been made in vain. Many thanks to my friends, new and old, but especially the ones that I made while in Durham. You all gave me a sense of community early in my time at Duke which made the harder times more bearable. I am truly blessed to be able to call you all my support system.

# 1. Introduction

Additive manufacturing (AM), commonly referred to as three-dimensional (3D) printing, has emerged as a transformative technology, enabling the production of highly complex structures that were previously unattainable with existing manufacturing methodologies. [13, 16] From AM comes the rise of lattice structures, which are lightweight structures with desirable mechanical properties and applications in several industries [2, 10]. They are designed using periodically repeating unit cells, which have geometric variability that allows the structures to meet specific mechanical or functional requirements, making them ideal for applications in fields such as aerospace, biomedical engineering, and mechanical design. While the use of these structures presents many opportunities for fast manufacturing and innovative solutions to existing problems, the mechanical behavior and fracture mechanisms in response to certain loading conditions remains an area of ongoing research [8, 10]. The lack of existing work done to understand the fracture behavior at a high level as well as its relationship to the parameters used to create the lattice structures results in uncertainty about the reliance on these structures and the potential risks towards client safety. Prior studies have explored the influence of variables such as porosity, print method, and material type as individual factors, yet research that puts these variables in conversation with one another is minimal.

Critical challenges in effectively utilizing AM lattice structures stem from their complex nature with mechanical properties not easily characterized by few numerical quantities. It is the dependency of their design parameters, such as material, unit cell, and print modality, that complicates the performance of these structures. The choice of material, whether it be a polymer, metal alloy, or composite, influences the failure mechanisms by altering properties such as fracture toughness, ductility, and crack propagation behavior. The porous nature of lattice structures also introduces stress concentrations that directly influence fracture behavior by

expediting crack nucleation and propagation. This results in significant uncertainty with fracture behavior, especially as the loading condition changes. [21, 35]

Traditional concepts in fracture mechanics like stress intensity factors provide a framework for understanding and predicting cracks, overall deformation, and strength under certain conditions. The interdisciplinary nature of fracture mechanics provides a natural curiosity for the mechanisms in AM; however, applying these principles to AM is difficult because of their heterogeneity and anisotropy. [27] These features result in fracture mechanics models that exhibit unique properties that are not traditionally observed with the homogeneous, bulk materials typically used in fracture mechanics. [10] In turn, the fracture surfaces of these lattice structures contain a significant amount of variability and non-linearity from required manufacturing methods. Accurately capturing and describing the full complexity of these exposed surfaces with imaging techniques like micro-computed tomography (micro-CT) and scanning electron microscopy (SEM), particularly in highly porous lattice structures, remains a challenge in the field.

Another potential related research area lies at the intersection of machine learning (ML) and AM. ML algorithms capable of pattern recognition and handling large datasets have the potential to aid complex fracture analyses by taking surface images and correlating them with the design parameters of the lattice structures. These algorithms can be extended to predictive models that are trained on existing data such that mechanical properties can be output as well as predictions of what fracture surfaces should look like when considering a combination of input parameters. [14] Despite these advances, there is still work to be done that encompasses fracture mechanics, AM, and ML for lattice structures. [19]

Schneider and Kumar [33] performed a study comparing the mechanical performance of lattice structures fabricated with three different printing methods and six different unit cells through uniaxial compressive loading and finite element analysis (FEA). This study was also

conducted with different lattice structure volumes and varying densities which proved to affect stretching or bending dominated structures. They reported that the simple cubic lattice structure had superior mechanical performance, namely through increased Young's modulus, strength, and energy absorption. Both the experimental and simulated FEA systems using multiple constitutive models showed variability in the stress-strain behavior exhibited by nonlinearities from brittle, viscoelastic, or plastic failure with regards to the layer-by-layer manufacturing process.

A 2023 paper by Nabavi-Kivi [27] also performs a fracture analysis of AM dogbone specimens in acrylonitrile butadiene styrene (ABS) material fabricated with fused deposition modeling. While these are not lattice structures, the study shows the impact of raster angle and layer orientation in the manufacturing process, which proved to have significant effects on the mechanical properties and fracture behavior of the dogbone specimens. Their findings included the anisotropy in Young's modulus, the ductile behavior observed from microscopy, and the crack deflection angle being related to the raster angle.

Wang et al. [36] provides a comprehensive review of machine learning applications in additive manufacturing. The article suggests ML being used in AM for the designing process by optimizing process parameters to accurately account for porosity, monitoring defects in powder-based printing methods, as well as planning the production process. More applications of ML in AM are expressed in Hooshmand et al. [19] where the researchers at the University of Regina used five ML algorithms to predict mechanical stiffness in simulated polymer lattice structures. Their results suggested that the combination of unit cell, cell size, and thickness as well as the complexity of the algorithm directly influenced the accuracy of predicting a strain model. The most important features were the lattice structure, thickness, Y, X, and Z configurations, respectively. The performance metrics showed that all the models had significantly low error values, with the artificial neural network outperforming the remaining models.

While these studies demonstrate significant interconnectivity across disciplines, there is still a gap in the literature pointing to a broader question about the feasibility of capturing and predicting fracture mechanisms in AM lattice structures with data science principles. This concept is hinged on the complex interplay of material properties, manufacturing processes, and geometric factors. The materials used in AM technologies, including elastic polymers, ductile metals, elastic-plastic composites, etc., introduces another level of complexity to the variability from exposed fracture surfaces. These materials display unique deformation and fracture behavior, with purely linear-elastic materials failing in a brittle manner, and ductile materials experiencing significant plastic deformation prior to failure. The variability that comes from ML model predictions, in combination with the inherent stochasticity of AM performance and failure mechanisms and with the wide array of materials in AM, proves that there is a growing need for integration of these concepts, where possible. This intersection of technologies has the potential to advance the understanding of how additively manufactured lattice structures behave under stress, ultimately leading to more robust and optimized designs for a wide range of applications.

### ***1.1 Objective***

The objective of this thesis is to analyze the fracture surfaces of additively manufactured cylindrical lattice structures fabricated utilizing multiple printing technologies, with the aid of machine learning algorithms. In doing so, the study would highlight an intersection of data science and additive manufacturing by validating what parameters in these prints are significant in the evaluation of fracture and mechanical performance. The study will compare ten materials over a range of six printing modalities. The structures themselves will have two defining characteristics: porosity and geometry of the repeated unit cell. The mechanical performance and subsequent fracture analysis will be determined by subjecting the samples to uniaxial tension. The goal of the ML aspect is to use the information from the fracture surfaces of the lattice structures after loading to predict a simulated fracture surface with feature importance.

## ***1.2 Thesis Outline***

The following chapters of this thesis will detail the intersection of additive manufacturing, fracture analysis, and ML in the outline that follows. Chapter 2 will highlight additive manufacturing in depth. The chapter will be broken up by the standard process for most technologies, followed by breakdowns of each printing modality being used in this study. The following section, Chapter 3, will specify additively manufactured lattice structures. It will highlight their applications in biomedical industries, various geometries, and their design by using different unit cells. Chapter 4 is *Materials and Methods*. This chapter will focus on the defining work for this thesis which comprises the design of the lattice structures, fabrication of the specimens, weight and porosity validations, mechanical characteristics, and imaging for fracture analysis. Chapter 5 will introduce the ML aspect of the study. The model architectures will be explained, in addition to the training and testing procedures and the metrics used for evaluating each model's performance. Chapter 6 will cover the results of the study. This will highlight the mechanical characteristics of the lattice structures discovered from mechanical testing, as well as the performance of the ML models. Chapter 7 will close the thesis with a discussion of the conclusions and findings in the study. Potential future work will be elaborated on.

## **2. Additive Manufacturing Technologies**

### ***2.1 Introduction***

As mentioned, additive manufacturing (AM) is a method of creating 3D objects that utilizes a layer-by-layer deposition technique [9]. There are several different print technologies that can be used to achieve the overall structure of the objects being made, especially for parts that may be more complex in nature. This chapter will break down the general process of AM but will also highlight the specific AM processes being used in this study. These manufacturing methods will be broken down into their specific operations and tasks which can also showcase the advantages and disadvantages of using certain methods at a given time.

#### **2.1.1 Process**

The general process of AM can generally be boiled down to six steps. However, the way in which these steps take shape will differ for each of the technologies. The six steps are as follows: 1) conceptualization and CAD, 2) file type conversion, 3) slicing, 4) machine set-up, 5) printing, and 6) removal with post-processing. The first step, conceptualization and CAD, prepares the entire print process by understanding and visualizing what object is desired to be manufactured. This requires the use of computer-aided design (CAD) for creating a digital 3D model of the object to be printed, or a pre-existing digital model of the part [9]. The next step is to convert the 3D model to the appropriate file type to be understood by the computer software that communicates with the printer. In most cases, this file type is the Standard Triangle Language, more commonly referred to as STL. Step three is slicing, the process of visualizing the 3D model as an STL on the build plate of the printer through a computer software designed to be understood by the actual printer. Slicing is where printing parameters such as the speed, material, size, and supports can be altered to impact the final quality of the print. These parameters may vary per printing style, as well as for each unique object being printed. As 3D printing is a layer-by-layer process, the completion of slicing shows the object as cross-sectional slices that build up to the

full part. This shows what each layer will look like and how the printer will operate to create the part. This slicing is then exported in an encoded structure that is understandable to the printer with a series of commands that communicates to the printer how to operate. Printing then begins, and the process is followed until the object is finished. The final step is removal and post-processing. This step entails removing the finished 3D object from the bed of the printer and any post-processing steps that may be needed. Post-processing for additive manufacturing often presents itself in the form of the removal of supports, sanding or finishing, washing, and/or heat treatments, and is highly dependent on the material used. Thermoplastic polymers may require sanding, photopolymer resins require washing, and powder-based materials can require hot isostatic pressing, machining, and surface coatings. The following subsections will further break down each printing modality being used in this study and will explain the variations from this overarching and broad representation of 3D printing.

## ***2.2 Material Extrusion***

Material extrusion is a form of AM that relies on material being loaded into a chamber to be liquefied and extruded through a nozzle to create the layers needed for fabrication. [13] The materials that can be used for this style of printing are thermoplastic polymers, ceramics, and liquid biomaterials. The extrusion aspect is dependent on these materials' ability to become liquid enough to be pushed through a nozzle. The extrusion mechanism can be pneumatic, screw-fed, can utilize a piston, or can utilize a feeding gear. The flow of the material through the nozzle is proportional to the pressure drop from the chamber to the atmosphere, as well as the nozzle geometry and the material's viscosity. As the material is being extruded, it will bond to the previous layer of material and will solidify prior to the next layer of molten material being extruded.

### **2.2.1 Fused Deposition Modeling**

Fused deposition modeling (FDM), sometimes referred to as fused filament fabrication (FFF), is a variant of material extrusion. FDM is the most common type of additive manufacturing and is what is often associated with the term 3D printing. [13, 24] The process for FDM works as described in the material extrusion introduction, with thermoplastic polymers as filaments and a feeding gear for the extrusion mechanism. This property of the polymer is important for creating adhesion between layers during manufacturing that solidify as needed at the conclusion of each layer deposited. [24]

### **2.3 Vat Photopolymerization**

The next form of AM is known as vat photopolymerization (VPP). This method involves the use of liquid photopolymer resins in a vat where the 3D object is created. [13] These photopolymer resins consist of a combination of liquid monomers or oligomers, reactive diluents, photo initiators, and additives as needed in the form of stabilizers or dyes. The process works by using a form of energy dependent on the photo initiator in the resin, typically gamma or ultraviolet rays, to polymerize the resin by breaking the oxygen double bonds present. This polymerization creates thermoset polymers that are chemically crosslinked which allows for the layers to bond to each other. At the completion of the printing process, the object is considered to be in a “green state,” [9] meaning that the layers and material are not fully reacted with one another. Due to this, VPP typically requires post-processing in the form of washing and curing. Parts are submerged in a solvent to remove any excess resin that remains on the outside of the print or inside any of the crevices, depending on the complexity of the part. Curing involves thermal or ultraviolet light exposure to the print, ultimately inducing further polymerization and increasing the strength and stiffness of the object. [26] The main variants of VPP technology are digital light processing (DLP), stereolithography (SLA), and mask projection (MPVP). The next subsection will cover DLP, the VPP method used in this study.

### **2.3.1 Digital Light Processing**

Digital Light Processing (DLP) is a variant of vat photopolymerization stemming from digital micro-mirror device (DMD) technology. [9] This technology uses a projected light source to polymerize the resin and cure cross-sectional layers. DLP differs from SLA by curing the full layer with the projector, as opposed to SLA using a laser to trace the contours of the layer. [26] The specific form of DLP used in this study is known as the bottom-up configuration, where the build plate is submerged in the resin bath and the part is inverted and manufactured upside down. [9, 32] This technology is beneficial in extending the range of materials that can be utilized in additive manufacturing and fabricates parts at a better resolution than material extrusion techniques.

### **2.4 Jetting Technology**

Jetting Technology is a class of AM that uses an inkjet print head to deposit material in droplet form. There are two sub-technologies that stem from jetting technology, material jetting and binder jetting. The material jetting process is similar to others in how it relies on layer-by-layer deposition techniques, but this method of printing propels liquid material that is dispensed from a nozzle, as opposed to extruding it like in material extrusion. The inkjet printhead comprises nozzles on the scale of thousands with diameters on the scale of microns. This allows the print material to be dispensed in small amounts at a very quick rate to print the object desired. The difference between material jetting and binder jetting is the material that is being dispensed. Material jetting dispenses the material that the 3D part will be made of while binder jetting dispenses a binding material into a bed of powder particles. These powder particles are what the final part will be made of, and the jetted material chemically bonds the powder particles together as needed.

### **2.4.1 Multi Material Jetting**

Multi Material Jetting (MMJ) is a form of material jetting technology that allows for the fabrication of parts with multiple materials. Droplets on the microscale are deposited in a similar layer-by-layer mechanism on a build plate. These materials are typically photosensitive resins that are much less viscous than in vat photopolymerization, or slurries that can be dispensed easily. [13, 16] The multiple printheads that are being used spray these materials and, due to this property, functional gradients can be created by using voxel scale design and associating materials with the voxels in the design software for these polymeric composites. [11, 16]

### **2.5 Laser Powder Bed Fusion**

Laser Powder Bed Fusion (LPBF) is an AM technology that relies on the utilization of a high-powered energy source in the form of a laser to fuse powder particles together to make a solid object in a layer-by-layer process. A rolling mechanism deposits powder particles onto a print bed to be fused together by the laser in the cross-sectional layers designed from the initial 3D model, and the amalgamation of these individual layers is what creates the 3D object made from the powder material. LPBF is the AM technology often used for the fabrication of many metallic parts and can be separated into multi jet fusion, selective laser sintering, and selective laser melting as specific print modalities.

#### **2.5.1 Multi Jet Fusion**

Multi Jet Fusion (MJF) is a technology under the umbrella term of LPBF. This technology introduced in 2016 comes from Hewlett-Packard (HP) and is used to produce high resolution, powder-based polymer objects. It uses a series of infrared lamps to fuse particles together by a jetted fusing agent. [7] This technology essentially combines the inkjet nozzle nature of jetting technology with the powder-based and fusing properties of powder bed fusion.

MJF also typically produces parts with higher ductility and smoother surface finish compared to other LPBF technologies and tends to be more efficient. [31]

### **2.5.2 Selective Laser Sintering**

Selective Laser Sintering (SLS) is a subset of LPBF that relies on the use of a high-powered CO<sub>2</sub> laser to sinter powder particles together with each other. [2, 13] Developed by Carl Deckard and Joseph Beaman at the University of Texas at Austin [6-7], the technology works by fusing powder particles at contact points without fully melting from a laser that scans the cross-sectional areas from each layer. [28] The build plate then adjusts to make room for a new layer and a thin, even layer of powder is spread using a roller or wiper blade for the next cross-section. While efficient and reliable, SLS has disadvantages by producing parts with rough surface finish that lack dimensional accuracy. [28]

### **2.5.3 Selective Laser Melting**

Selective Laser Melting (SLM) is essentially the same process as SLS; however, this process utilizes melting of the powder particles in their fusion, which ultimately allows for metals with higher melting points to be printed with. SLM uses a high intensity laser as its energy source but can be replaced by an electron beam for a different form of powder bed fusion with melting. [20] During SLM, the build area is typically enclosed and filled with gas to facilitate an inert environment that prevents oxidation. [38] Parts are fabricated on a metal print platform and require the use of a bandsaw or electrical discharge machining (EDM) to separate the parts from the build plate. Unlike SLS, supports are needed in the SLM process because of warping that can occur from the melting of the materials used. SLM is superior to other LPBF technologies because the melting aspect allows the production of fully dense objects, thus enhancing the manufacturability of these metallic parts. [38]

## ***2.6 Chapter Summary***

This chapter details the general process of additive manufacturing. It explains the types of additive manufacturing processes with specific technologies that fall under each process. The specific technologies highlighted are used in this study for the fabrication of lattice structures, and are discussed more in the subsequent chapters.

## **3. Additively Manufactured Lattice Structures**

### ***3.1 Introduction***

Lattice structures are in high demand because of their high strength-to-weight ratio and favorable mechanical properties. [15, 23, 29-30] These structures traditionally pose considerable challenges in manufacturing; however, advancements in engineering processes, more specifically AM, make it possible to fabricate these structures that are defined by their intricacies, complex geometries, and their periodicity with significant accuracy. [14] While AM is beneficial to this end, another hindrance in the manufacturing process with these technologies lies in the consideration of minimum feature size. Each AM process will have limitations based on the physical components of the printer that affect their resolution. In turn, some unit cell geometries are not feasible to fabricate with sufficient precision. [23] Nevertheless, at a base level, AM allows for successful fabrication of these parts, with flexibility in geometry and porosity in their initial design.

### ***3.2 Applications***

Due to their desirable mechanical properties, lattice structures have uses in several industries. [10] Khan et al. [23] explains the use of these structures in the aerospace and aviation industry. In this field, AM components are commonly manufactured with LPBF methods because of the robust nature of metallic or high-strength polymeric prints. More specifically, they explain that AM lattice structures can be used for vehicle engines, cooling structures, combustion chambers, and brackets. This range of application within one industry is because of the flexibility that comes with designing and producing these structures such as infill density, conformation, and unit cell. AM lattice structures have also been used in airplane wings as explored by Spadoni et al., which suggested that lattice structures can endure significant deformation prior to total failure. [34] While these are specific applications of AM lattice structures, generally, lattice structures prove to be sufficient in applications where stiffness, energy absorption and high specific strength

are needed in addition to the benefit of being lightweight. [2-3] This extends out of aerospace and into automotive, energy, and biomedical industries as well. [9, 25]

### **3.2.1 Biomedical Implants for Bone Regeneration**

A primary application of additively manufactured lattice structures is in biomedical implants [2, 21], particularly for bone regeneration. This implementation hinges on the principle of osseointegration, a concept referring to the biological interactions between bone tissue and a load bearing implanted material. [12, 18] This process facilitates bone growth at the site of the implant, allowing for structural fusion between the tissue and implant to enhance the structural integrity and stability of the areas with fracture or limited bone density. Initially prevalent in dentistry, developments in AM make space for the fabrication of more complex and intricate geometries with a larger size range to be utilized as implants, thus expanding the exploration of these implants to other areas of the body. These load bearing implants are predominantly constructed from metal alloys, with titanium being the typically favorable option because of its biocompatibility and superior mechanical characteristics. [8, 17-18, 25]

The complex nature of lattice structures is directly linked to their inherent porosity. This feature plays a large role in their effectiveness as implants because it not only allows the bone to fuse to exposed surfaces of the implant, but also facilitates ingrowth through the pores in the structure, largely creating a supportive scaffold for bone regeneration. Additionally, the pore shape and size are largely influential on the osseointegration and stability of the implant. These implants can be printed with functionally graded materials, which gradually vary in composition and allow for reduced stress concentrations. [25] This is significant because the implementation of these materials and adjusted pore parameters can optimize the stress distributions between bone and implant faces [5], improve bone resorption [4], and reduce stress shielding. [1, 25] This precision and control that AM technology provides further enables the evaluation and integration of 3D printed structures to progress medical technologies and favorable patient results.

### **3.2.2 Geometry**

With the novelty of AM and the increase in industry demand for lattice structures, the geometric configuration of these structures is often in question and primed for adaptability across applications. Lattice structure industrial implementations have historically relied on cubic geometries due to their relative simplicity and ease of integration. These parts were less difficult to fabricate because of consistency across dimensions, and in pressurized or load bearing instances, these parts would likely display uniformity with stress distribution. Naturally, this geometry cannot be defaulted to in every instance where a lattice structure could be useful, and advancements in AM continue to make it possible to consider these structures with cylindrical, spherical, and conical geometries. Spherical structures may be needed for cases regarding energy storage or pressure containment [8], which can similarly provide uniformity in stress and load distributions while entirely changing configuration. Cylindrical and conical structures may be used as functional components in aerospace or automotive projects [25], where a higher level of precision may be needed for optimization of the vehicle. The biomedical implants in the previous section are often made as customized structures unique to each patient that cannot fall into a specific geometric category. [25] This evolution of geometry has led to the incorporation of a more diverse set of unit cell configurations that inherently define the lattices, which in turn offer superior strength and functionality needed for expanding industrial applications. [8]

### ***3.3 Unit Cells***

Unit cells are the fundamental components of lattice structures, effectively defining the periodicity that these structures are known for. This periodicity and other unit cell parameters directly affect the functionality and mechanical characteristics of the structure by determining its internal architecture and densification patterns. [23] Several unit cell geometries exist, ultimately giving rise to customization and variability within these lattices to adjust for the necessary

applications. These unit cells can be separated into multiple categories, but generally can be characterized as either “strut-based” or “sheet-based”.

### 3.3.1 Strut-Based Unit Cells

Strut-based unit cells are composed of interconnected struts that form the lattice architecture. These interconnections are modeled as trusses, where the individual struts meet at various nodes throughout the structure. It originates from the simple cubic unit cell and is mathematically defined using a coordination number that refers to the number of neighboring struts connected to a singular node. One of the more well-known strut-based unit cells is the octet-truss, which is highlighted throughout this study and is defined with a coordination number of 12. Figure 1 below shows example strut-based unit cells, with the octet-truss shown in D.

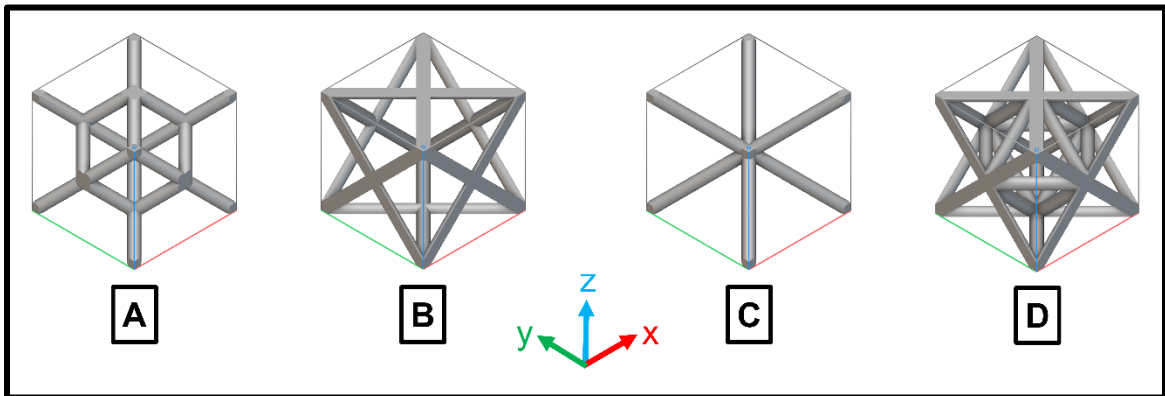


**Figure 1: Strut-Based Unit Cells.**

A) Fluorite. B) Face-Centered Cubic. C) Body-Centered Cubic. D) Octet-Truss.

### 3.3.2 Sheet-Based Unit Cells

Sheet-based unit cells are defined by continuity as demonstrated by the surfaces on these sheets. These unit cells are often referred to with the term triply period minimal surface (TPMS), which suggests a minimal surface area for a given volume of the unit cell. A prominent example of this type of unit cell is the gyroid, which is comprised of three sinusoidal waveforms in 3D space with connected surfaces that provide favorable mechanical properties. [2, 14, 18] Example sheet-based unit cells are shown in Figure 2, with the gyroid and its defining equation expressed.

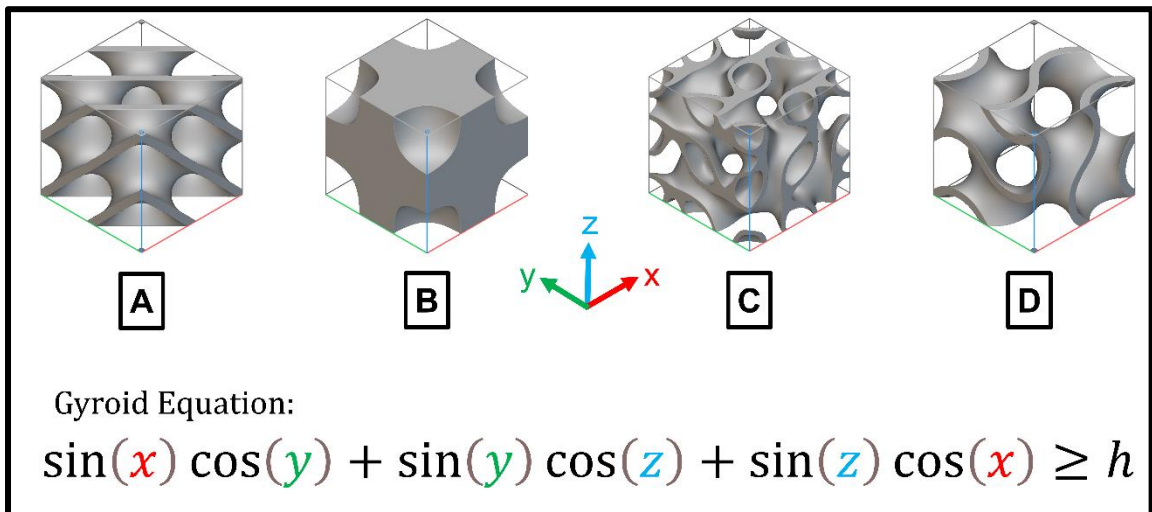


**Figure 2: Sheet-Based Unit Cells.**  
A) Diamond. B) Neovius. C) Lidinoid. D) Gyroid.

### 3.4 Chapter Summary

This chapter delves into the specific application of additive manufacturing in this study with the topic of AM lattice structures. It discusses general uses for the structures, with a focus on lattice structures as biomedical implants for bone regeneration and osseointegration. The chapter also considers the role of geometry in these lattice structures, with a section on the properties of different unit cells and the introduction of the overall shape and unit cells being tested in this study.

## **4. Materials and Methods**

### ***4.1 Introduction***

The following chapter details the materials and methods used in the development of this study. It explains how the lattice structures were designed initially as digital 3D models, the fabrication and printing process for the different technologies, and the mechanical testing procedures. That is followed by the imaging techniques used to transition into the ML component of the research.

### ***4.2 Lattice Structure Design***

Lattice structures are designed in nTopology, an implicit design platform. This software works by using block-based coding to perform sequences in design or analysis. The dimensions of a solid cylinder are set with a diameter of 12 millimeters and a height of 18 millimeters, and the built-in volume lattice and cell map commands are used to create porous and periodic objects. Unit cells can be imported and selected from a list to create the structures as desired. CAD files of solid tabs designed in SolidWorks are imported and a Boolean intersect is used to combine the lattice with the solid tabs as needed for the grips on the mechanical testing machine. This implicit body is meshed and exported as a 3MF file to be used with the various printing software.

#### **4.2.1 Unit Cells**

As discussed in section 3.3, a sufficient distinction of unit cells lies between strut-based and sheet-based forms. For this study, the strut-based unit cell being used is the octet-truss and the sheet-based unit cell is the TPMS gyroid. These two distinct unit cells are standard in existing literature for the respective unit cell types and would provide a vast amount of information regarding mechanical properties and fracture response.

## **4.2.2 Porosity**

In addition to the change in unit cell, variations within the individual lattice structure designs are most evident through the change in porosity. In this line of work, porosity is periodic and defined as the void space within the lattice. [29-30] As mentioned, pores in these lattice structures facilitate bone regeneration when used in the context of biomedical implants; therefore, four porosity values are being examined through this study. Parts are designed to range from 50% to 80% porosity in increments of 10% [50, 60, 70, 80]. By adjusting the wall thickness, this effectively changes the porosity in the prints, causing stark changes in the mechanical performance of the lattice structures.

## ***4.3 Fabrication of Cylindrical Lattice Structures***

After the structures are designed in nTopology, they are exported in the necessary file types to prepare them for slicing and printing. Parts are arranged on build plates in various slicing software for the respective printing methods and mass manufactured in batches until the total number of samples are produced with high quality. Printing parameters such as supports, print speed, bed adhesion, etc., are altered as needed. The orientations and layer height of all structures are held constant which allows for a more direct comparison. Post-processing steps are utilized for certain printing methods following the completion of the printing process as mentioned in Chapter 2. Due to the concept of minimum feature size introduced in Chapter 3, some of the designed structures could not be fabricated due to limitations of the machinery. For these lattice structures, wall thickness is the feature that typically sets a threshold of what can and cannot be printed successfully. For some of the printing methods, the wall thickness of higher porosity samples was too small, and those parts could not be printed.

In addition to the lattice structure samples, solid dogbone samples are made for normalized strength comparisons between solid and lattice. These solid samples differ in geometry from the lattices as they are designed per the ASTM-E8 standard for metallic specimens

under tensile testing. These are used for the primary purpose of efficient mechanical tests that provide the mechanical properties of each material demonstrable with stress-strain curves. A different set of solid parts that combine to resemble the geometry of the lattice structures with the same dimensions are also fabricated with the same materials and print methods as mentioned.

Unlike the samples being mechanically evaluated, these solid parts are not made as full dogbone samples, but instead are manufactured as separate parts of solid cylinders and solid tabs. These parts serve the purpose of porosity validation, which will be described in subsection 4.4.

Figure 3 at the end of this section shows the CAD renderings and fabricated samples of the lattice structures for all materials at 50% porosity and the solid specimens. This is followed by Table 1, documenting the properties of each material in this study.

### **4.3.1 Fused Deposition Modeling**

The lattice structures manufactured using FDM are fabricated at Duke Chesterfield Lab using a Bambu Lab P1 Series printer. The materials used with this modality were polylactic acid (PLA) and polyethylene terephthalate glycol (PETG) in filament form, both supplied from Bambu Lab. PLA and PETG are commonly used polymers for FDM fabrication. In the Bambu Studio slicing software, lattice structures are segmented into three groups: bottom tab, lattice, and top tab. Printing parameters such as decreased layer thickness, slower infill speed, and larger infill density are adjusted for the lattice section to aid the machine in the creation of the complex structure. Prior to fabrication, a liquid adhesive is applied to the build plate for batches using either material. This ensures that parts do not detach from their supports on the print bed as the printing process occurs. The printing process is continuously monitored to ensure the successful completion of the printing process that is often hindered by the accumulation of excess filament adhering to the nozzle. This usually results in clogs, damage to the machine, and/or obstruction of the lattice structure prior to its finish. For 50% through 70% porosity samples, a stainless-steel nozzle with diameter equal to 0.4 millimeters is used. For the 80% porosity samples, this nozzle

is switched to a 0.2-millimeter diameter to aid the smaller features. This process is successful for PLA; however, the prints in PETG material failed. No post-processing steps are needed for either material for this process.

### **4.3.2 Digital Light Processing**

Lattice structures manufactured by DLP are fabricated at Chesterfield using a 3DSystems Figure 4 Standalone printer. DLP prints are made using Tough Grey 15 (TGR) and Tough Clear (TCL) resins by 3DSystems. DLP structures are set up directly on the build plate without supports. Post-processing in the form of washing and curing was needed for this technology. Parts are removed from the build plate at the conclusion of the printing process and immediately submerged in isopropanol for twelve to fifteen minutes to wash off excess resin inside of the pores of the lattice, as well as on the exterior of the part. Parts are then exposed to thermal and ultraviolet curing using a Formlabs Form Cure. TGR parts cure at 60°C for 30 minutes and TCL prints cure at 35°C for 25 minutes.

### **4.3.3 Multi Material Jetting**

MMJ prints are fabricated by Duke University Bluesmith using a 3DSystems MJP2500 printer in the VisiJet M2R-CL material (abbreviated as VJC).

### **4.3.4 Multi Jet Fusion**

The parts made using MJF technology are outsourced and manufactured by JawsTec using HP MJF technology. These parts are fabricated with both Nylon-11 and Nylon-12 materials.

### **4.3.5 Selective Laser Sintering**

SLS parts are also outsourced and manufactured by JawsTec using Nylon-11 and Nylon-12. While these are the same materials as MJF by convention, their material properties are not identical as they are manufactured using different processes.

### **4.3.6 Selective Laser Melting**

The last printing technology, SLS, is used to manufacture the cylindrical lattice structures in the titanium alloys Ti6Al4V. This method is performed at the Duke University Foundry using a 3DSystems ProX DMP320 metal printer.

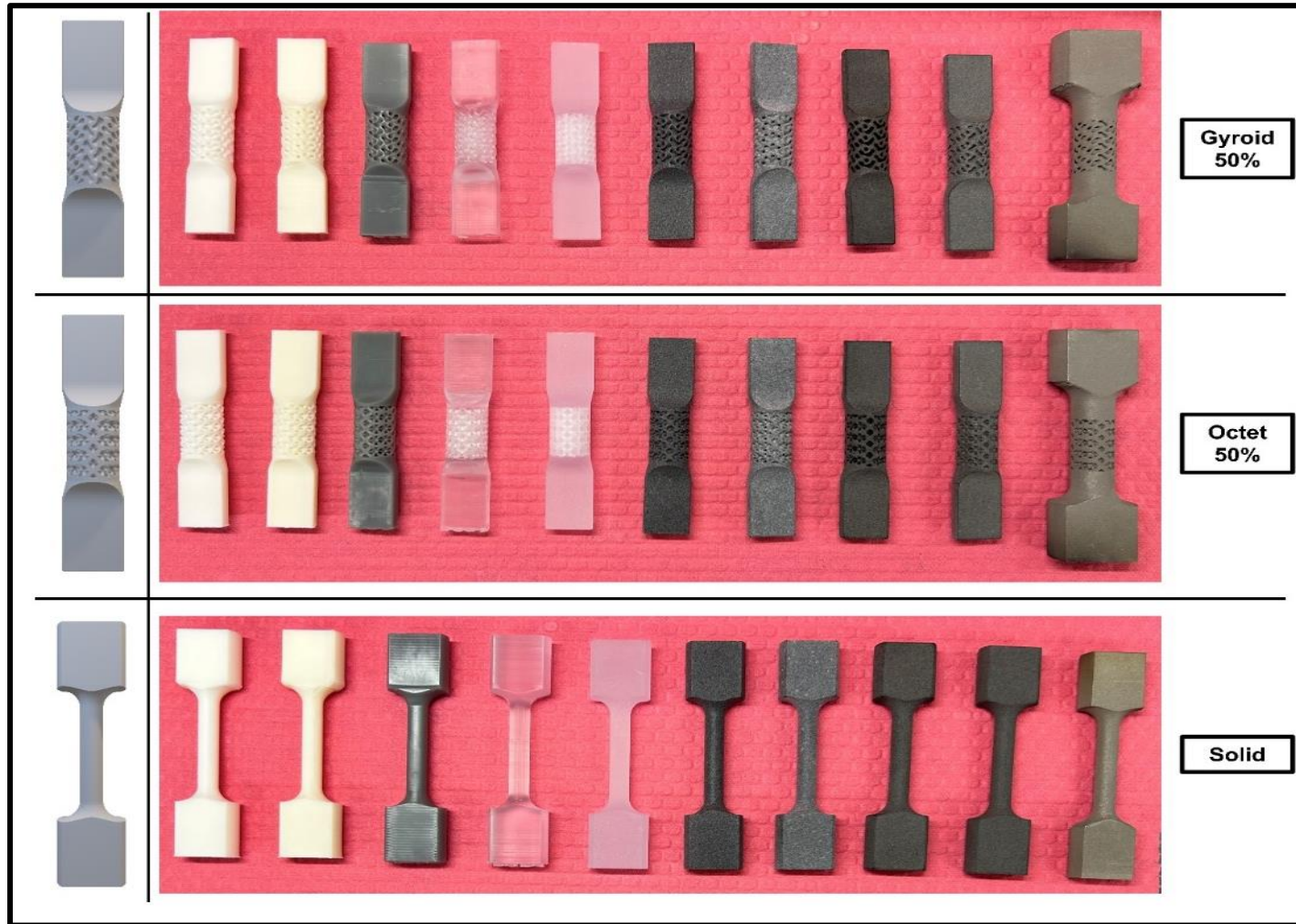


**Figure 3: CAD Renderings and Printed Samples for 50% Porosity Lattices and Solid Structures.**

From left to right: FDM – PLA, FDM – PET, DLP – TGR, DLP – TCL, MMJ – VJC, MJF – N11, MJF – N12, SLS – N11, SLS – N12, SLM – T64

**Table 1: Material Properties**

Technology	Material	Young's Modulus [MPa]	Ultimate Tensile Strength [MPa]	Strain at Break [%]
FDM	PLA	2580	35	12.2
	PET	1650	45	24
DLP	TGR	2120	48	35
	TCL	2300	52	12.3
MMJ	VJC	2200	50	11
MJF	N11	1800	52	40
	N12	1800	48	15
SLS	N11	1550	48	40
	N12	1725	48	21
SLM	T64	122000	980	14

#### 4.4 Porosity Validation

After all samples for a given print technology are complete, a weight-based approach is used for porosity validation. Three samples of each lattice structure, considering technology, material, porosity, and unit cell are weighed and averaged. The same strategy is used for the solid cylinder and solid tabs that resemble the shape of the dogbone lattice samples.

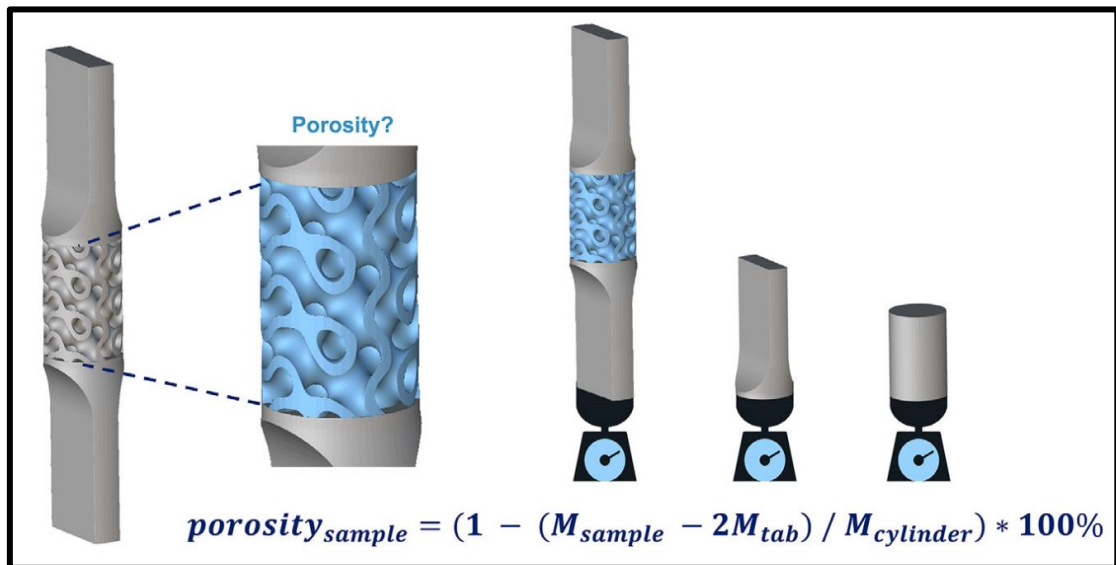


**Figure 4: Weight-Based Porosity Validation Process.**

[29-30]

## 4.5 Mechanical Characterization

To evaluate the mechanical performance of the printed structures, polymeric parts are tested using a TestResources 830LE63 Axial Torsion Testing Machine via Duke University and metal lattices are tested at restor3d, an additive manufacturing company focused on orthopedic solutions in Durham, North Carolina. See the test setup in Figure 5 below. Both lattice structures and solid structures are subjected to uniaxial tensile tests at a 1 millimeter/minute testing speed with a 10000 pound-force load cell. The direction of the tests is perpendicular to the print orientation of each structure. Each sample group is tested with a minimum of three duplicate samples to account for variance.

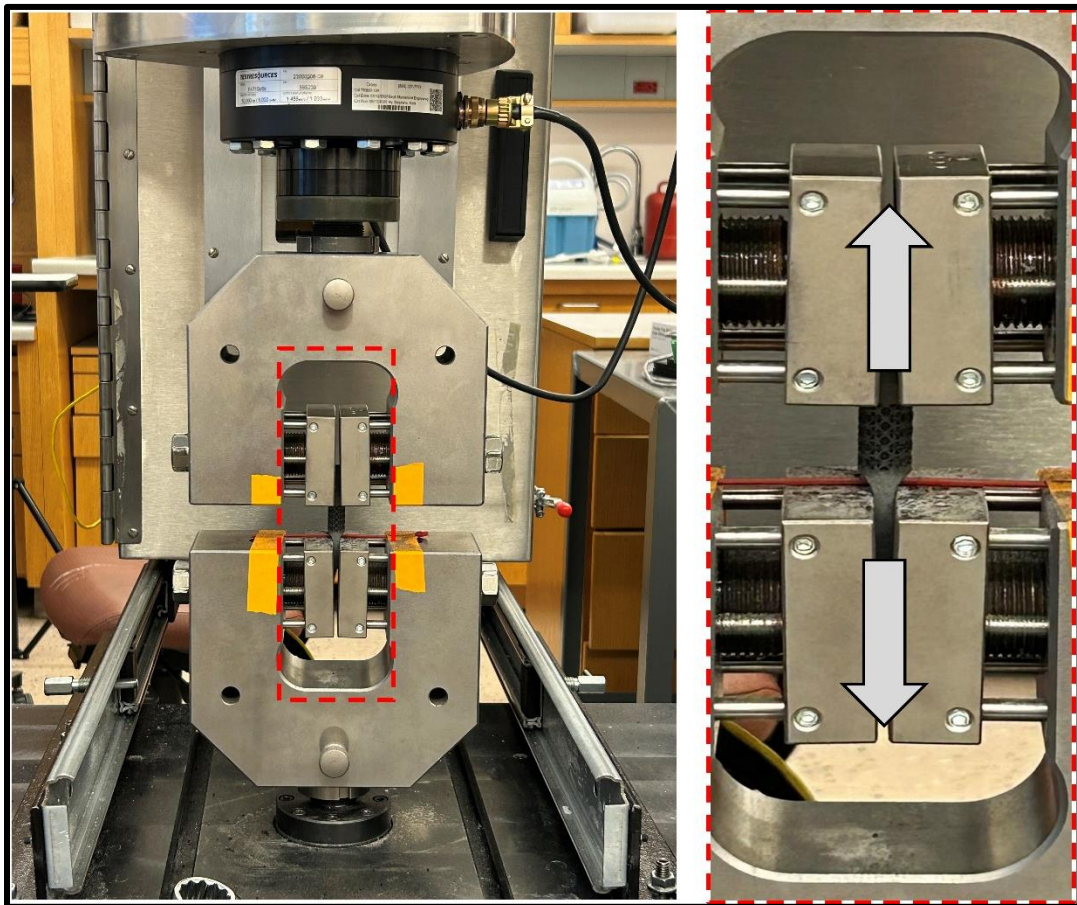


**Figure 5: Mechanical Testing Setup.**

Left) Full testing frame. Right) Magnified Testing Frame with Loading Direction Denoted.

## ***4.6 Microstructural Imaging for Fracture Analysis***

To analyze the fracture surfaces of these lattice structures, imaging techniques need to be used to highlight print imperfections, defects, and deformation on the micro- and nanoscales. Observing these effects will not only show where cracks begin and how they propagate throughout the rest of the print, but also where the printing technology failed to be precise, ultimately affecting its porosity and fracture mechanics. This study relies on both scanning electron microscopy (SEM) and micro-computed tomography (Micro-CT) for further understanding of the parts post mechanical testing.

### **4.6.1 Scanning Electron Microscopy**

SEM serves as a tool for identifying defects, print imperfections, and microscale deformation on the fractured surface of each structure. The process works by the interaction of an electron beam with the sample. Electrons are targeted towards the structure and a greyscale image is generated based on the electrons that hit the surface and the electrons that bounce back from the surface towards the gun. The images can be adjusted by the introduction of the Trinity detectors, three detectors that alter the way the beam interacts with the surface. These detectors can emphasize surface and boundary conditions, material composition, and/or large defects in the sample.

SEM in this study is performed using a ThermoFisher Scientific Apreo S Scanning Electron Microscope with EDS Detector from the Duke University Shared Materials Instrumentation Facility (SMiF). Fractured lattice structures are adhered to orthogonal sample stubs that oriented the samples vertically such that the fracture surface is exposed in its entirety under the electron beam. Only certain samples are imaged using SEM to show general trends across print methods and unit cells. Additionally, SEM takes images with higher quality and efficiency for parts that are made of conductive materials. Due to this notion, certain materials need to undergo a sample preparation process in the form of sputter coating. Sputter coating, also

called gold sputtering, is the process in which a thin gold film is sprayed onto a material to make the sample conductive. In the case of these lattice structures, sputter coating is used for the polymeric materials from the FDM, DLP and MMJ technologies primarily. This sample preparation process is also attempted for SLS prints but because of the powdery nature of these samples, the spraying mechanism tends to push out excess powder particles, thus limiting the adhesion of the gold film to the fracture surface.

Few parameters are adjusted during imaging with SEM to increase the quality of the images and highlight certain aspects of the lattice structures. This included the magnification range, which stays between 46x and 2000x, and the detectors used, which include the Everhart-Thornley detector and the T1 and T2 Trinity detectors. The dwell time of 300 nanoseconds, the scan resolution of 1536 x 1024, the accelerating voltage of 2 kilovolts, and the emission current of 25 picoamps are mostly standard parameter values for SEM.

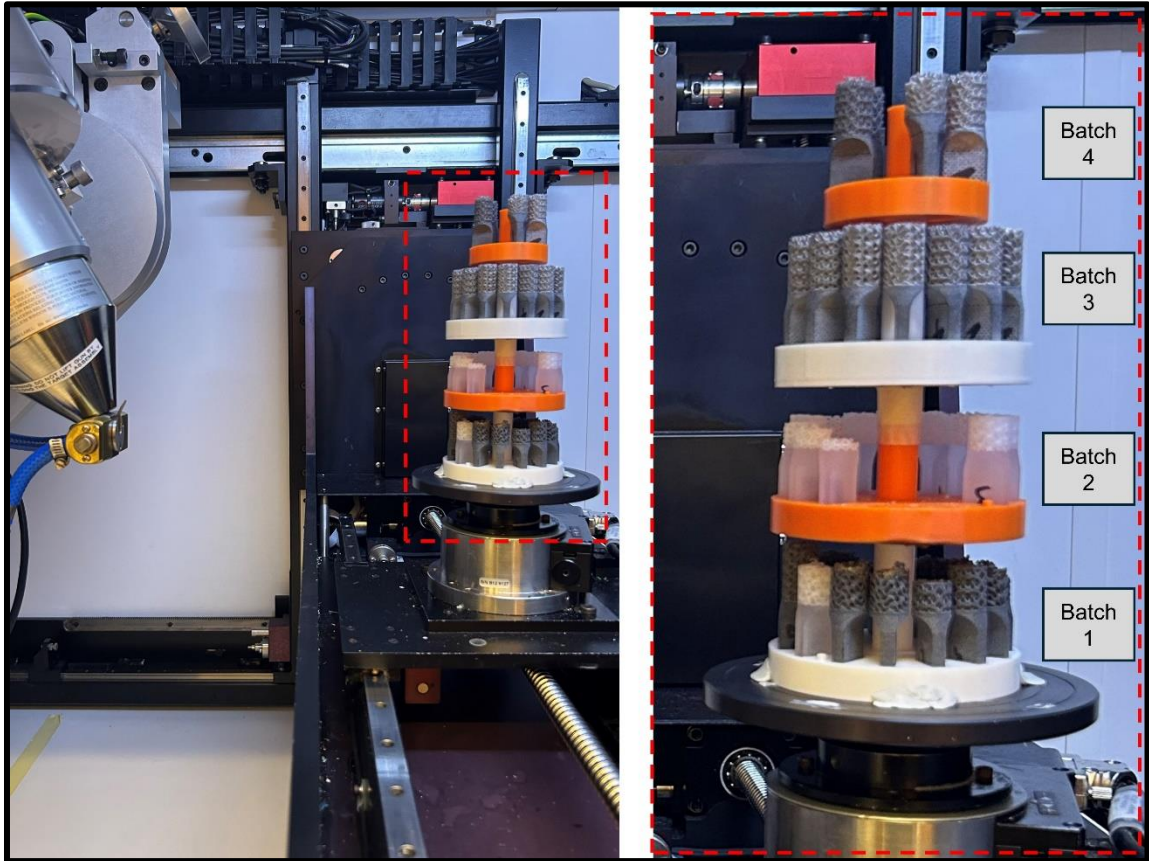
#### **4.6.2 Micro Computed Tomography**

Micro-CT is used as the primary imaging technique for identifying the topography in the fracture surfaces. This imaging process, as opposed to SEM, allows for a volumetric analysis of the entire print, which can then be used to generate 3D reconstructions of the part as STL files that can be converted to meshes and point clouds to define the fracture surfaces in a format easily digestible for data in an ML algorithm.

This imaging is performed using a Nikon XTH 225 ST High Resolution X-Ray Computed Tomography Scanner courtesy of Duke SMiF. Broken lattice structures are arranged vertically on their solid tabs in the same orientation by being slotted into a 3D printed holder to allow for mass scanning. Two fractured samples are imaged for each unique design. These parts are stacked on top of each other to facilitate batch scanning, a process in which Micro-CT can be

programmed to move between individual levels. This CT setup with the 3D printed lattice holder for batch scanning is seen in Figure 6.

**Figure 6: Micro-CT Setup for Batch Scanning of Fractured AM Lattice Structures.**



The parameters adjusted with this form of imaging are used to optimize the image as the varied materials could affect contrast and resolution. Beam energy is typically set in the range of 140 to 180 kilovolts due to the higher density of the materials. Power is set based on the effective pixel size which is determined from the magnification used when ensuring that all the lattice structures being imaged at a given time fit within the bounds of the frame of view. This value generally exists between 40 and 50 Watts. Exposure time is short because of the high energy and dense samples that are being used, therefore, a range of 267 to 354 milliseconds is set. In the reconstruction phase of imaging, the beam hardening parameter is set to a value of two. In the final step, the shading correction parameters of frames to average, number of images, and white

target are set to values of 300, 3, and 60000, respectively. The projections are optimized which results in a value of 3141 with 2 frames per projection.

The analysis is aided by the ImageJ software for viewing the layers and internal structures as shown by the scan. Each individual lattice structure is segmented from an image sequence stack, brightness and contrast are adjusted, the solid versus the pore is binarized, and it is then converted into a 3D reconstruction of the part as an STL file using the 3DViewer plug-in. This allows the tested prints to be viewed digitally, giving way to mathematically defining the plane covering the fracture surface. These mathematical coefficients are then used as the basis for training and testing datasets in the ML algorithms.

#### ***4.7 Chapter Summary***

Chapter 4 covers at length the materials and methods of the research. This chapter shows the detailed process of fabricating each sample and how those processes may be altered by printing modality. It explains the process of mechanical testing as well as the imaging tools used. The following chapter begins to explain the machine learning aided fracture analysis.

## **5. Machine Learning Model and Theory**

### ***5.1 Introduction***

The next phase of the study introduces the role of data science principles in the form of machine learning. This section breaks down the process for how the fractured AM lattice structures are converted into understandable digital information, processed, and manipulated to determine the plane best fit to the fracture surface. This sets up the use of multiple machine learning models, which will be elaborated on towards the conclusion of the chapter.

### ***5.2 Code Breakdown***

#### **5.2.1 Preprocessing and Initialization**

Before the ML component of the study can be performed, the STL files of the fractured lattice structures need to be processed and correctly associated with their defining characteristics. This allows for information from ImageJ to be digested and suitable for ML. This section of the project was completed in Python using Visual Studio Code (VSCode).

The process starts with importing the necessary libraries related to meshing, plotting, model selection, and metrics. A material library is then defined to associate the individual materials used with their respective print technologies and their Young's modulus, strain at break, and ultimate tensile strength, as defined in Table 1. Before loading the STL files into VSCode, the initial files created from the ImageJ software are run through a mesh reduction sequence made in nTopology to reduce the resolution of the fractured lattices. This makes processing the files more efficient as their size decreases by magnitudes of up to six. These reduced STL files are then pulled from each corresponding folder and processed to extract the information from the filename. The naming convention is 14 characters that comprise information about print technology, material, unit cell, and porosity (ex: FDM\_PLA\_G80\_04 is a lattice structure fabricated using FDM, PLA material, the gyroid unit cell, 80% porosity, and was the fourth

sample tested of this configuration.) These features are stored as inputs and converted to numeric values.

### 5.2.2 Defining Fracture Surfaces and Plane Fitting

The next part of the code is a significant preparatory step for ML, which is the definition of each individual fracture surface and the fitting of a fourth order plane to said fracture surface. The STL files that are imported are transformed into meshes which are used to generate point clouds of the lattices. The point cloud is then separated into a 30x30 grid, where it locates and marks the largest Z-value in each cell. Different grid sizes are experimented with between 5x5 and 50x50. 30x30 is ultimately selected based on efficiency and where results started to plateau. A maximum radius is also set based on the relative size of the structures to bound the infinite plane so that inaccuracies from edge effects for insignificant points or noise generated in the point cloud are reduced. This leads to the formation of a polynomial surface fitting function that uses the highest vertical point in each cell, fits a surface of desired order to these points, and returns the coefficients of the plane of best fit. Considering that these are three-dimensional objects, a fourth order plane is used, yielding 15 coefficients. These coefficients are matched with their respective structures and stored. Figure 7 is a flowchart depicting the process explained in this subsection.

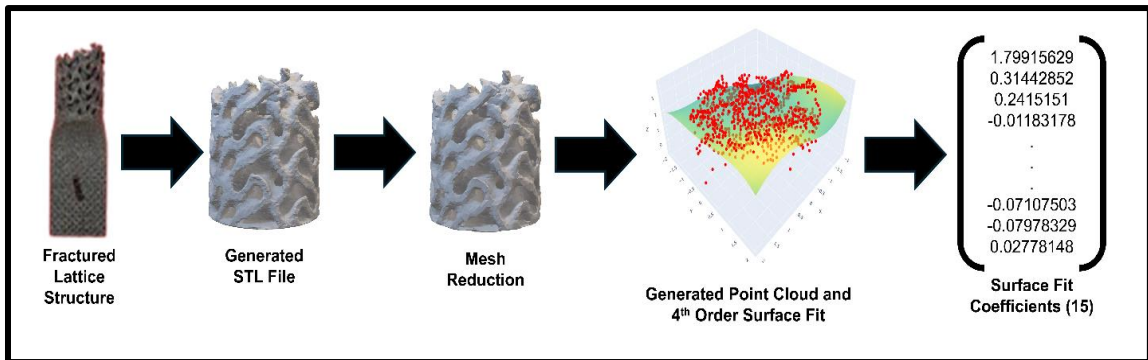


**Figure 7: Process for Defining Fracture Surfaces and 4<sup>th</sup> Order Plane of Best Fit.**

## ***5.3 Machine Learning Setup***

### **5.3.1 Inputs and Outputs**

The inputs of the ML algorithms match with the filename information extracted from earlier. These models use Young's modulus, strain at break, ultimate tensile strength, porosity, unit cell, and print method. The primary output of the study is the predicted surface coefficients. The model uses a randomized 80:20 train/test split where the dataset is comprised of the surface coefficients determined in 5.2.2.

### **5.3.2 Principal Components Analysis for Feature Reduction**

The performance of the ML models ties to its complexity, which is largely defined by the need to accurately predict 15 different coefficients for many samples. To simplify this, principal components analysis (PCA) is used as a feature reduction technique to limit the number of coefficients needed to accurately describe the fracture surface. To determine the best number of coefficients to reduce to, an explained variance plot is used. This plot shows the percentage of variance being explained against the number of coefficients needed, which can allow for user discretion on the amount of variance needed and potential tradeoffs for using fewer components. Based on this plot shown in Figure 8 below, 10 principal components correspond to the same amount of variance explained for the initial 15. Reducing this number results in a model that

captures the same amount of data in a way that is less difficult for each algorithm to understand and attempt to compute.

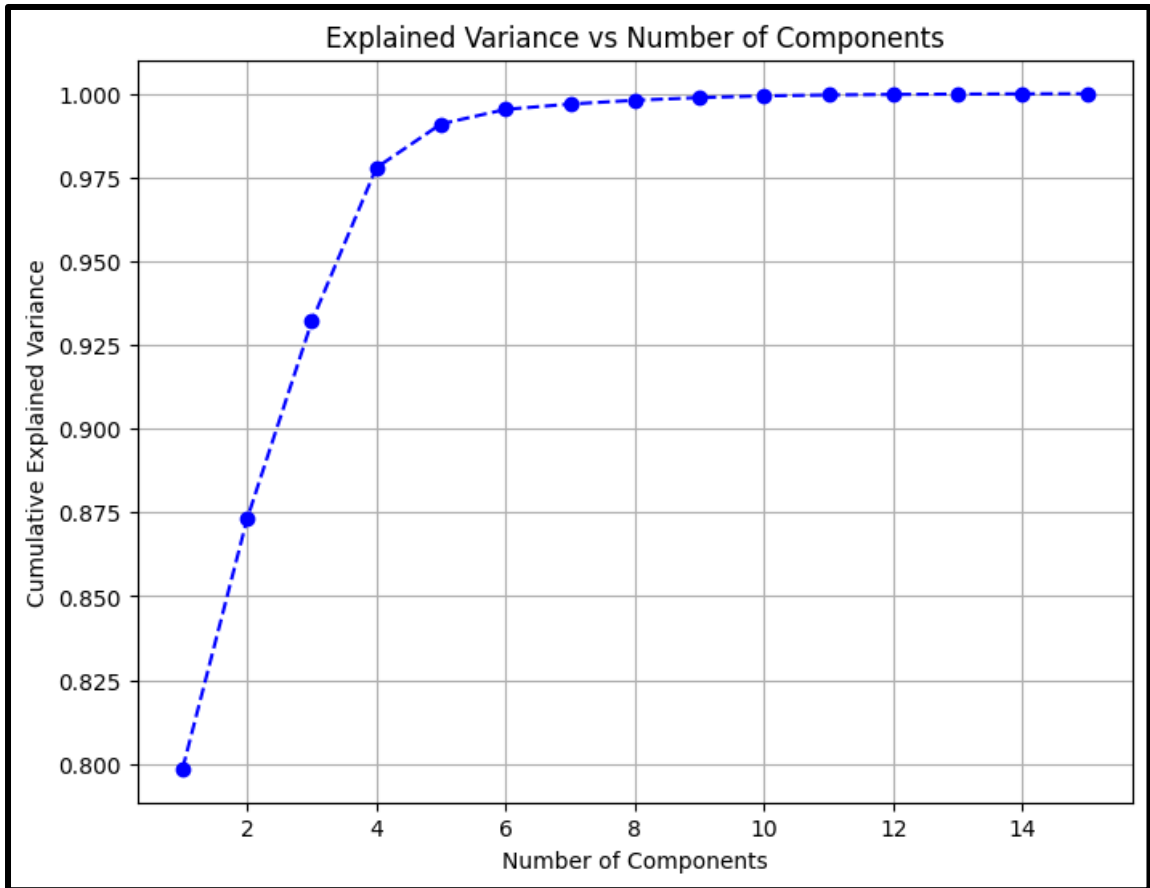


Figure 8: Explained Variance vs Number of Components.

## 5.4 Model Architecture for Algorithms Used

### 5.4.1 Kernel Ridge Regression

The first model being used for predicting the fracture surface of the lattice structures is Kernel Ridge Regression. This algorithm is a form of penalized regression that works by using the L2 norm and is used when most inputs are relevant, but correlation instability should be avoided. This model reduces overfitting and can kernelize data for large dimensions with simplicity and high predictability [19, 29-30]. This model provides a baseline in terms of model complexity relative to the remaining three models that will be used.

As mentioned, an 80:20 train/test split is used for all models. In terms of hyperparameters for this algorithm, the kernel selected was the radial basis function and the regularization alpha parameter was set at 0.01. The radial basis function kernel and alpha hyperparameter value were selected because they performed the best with respect to the other combinations, in large part because of their ability to handle non-linearity and their simplicity.

### **5.4.2 Polynomial Regression**

Polynomial Regression is the second algorithm being tested in this study. This model is also a standard regression that defines the relationship between the independent variables and the dependent variables with an n-degree polynomial. This model could be beneficial to use to predict the fracture surface of the AM lattice structures because the surface fit is being completed with a fourth order polynomial. [19] This might make it easier since the entire dataset is dependent on this surface fit, and a polynomial predictive model would likely predict polynomials in the test dataset with higher accuracy. The primary parameter that affects the architecture of this model is the order of the polynomial being used to define the relationship of features to targets.

### **5.4.3 Random Forest**

Random Forests are another form of regression analysis that operates with the construction of multiple layers of decision trees. This model is also very simple in nature and introduces randomness to reduce the correlation between decision trees. This ultimately improves the performance by reducing overfitting. [19] In this study, the number of decision trees being used is set at a value of 100.

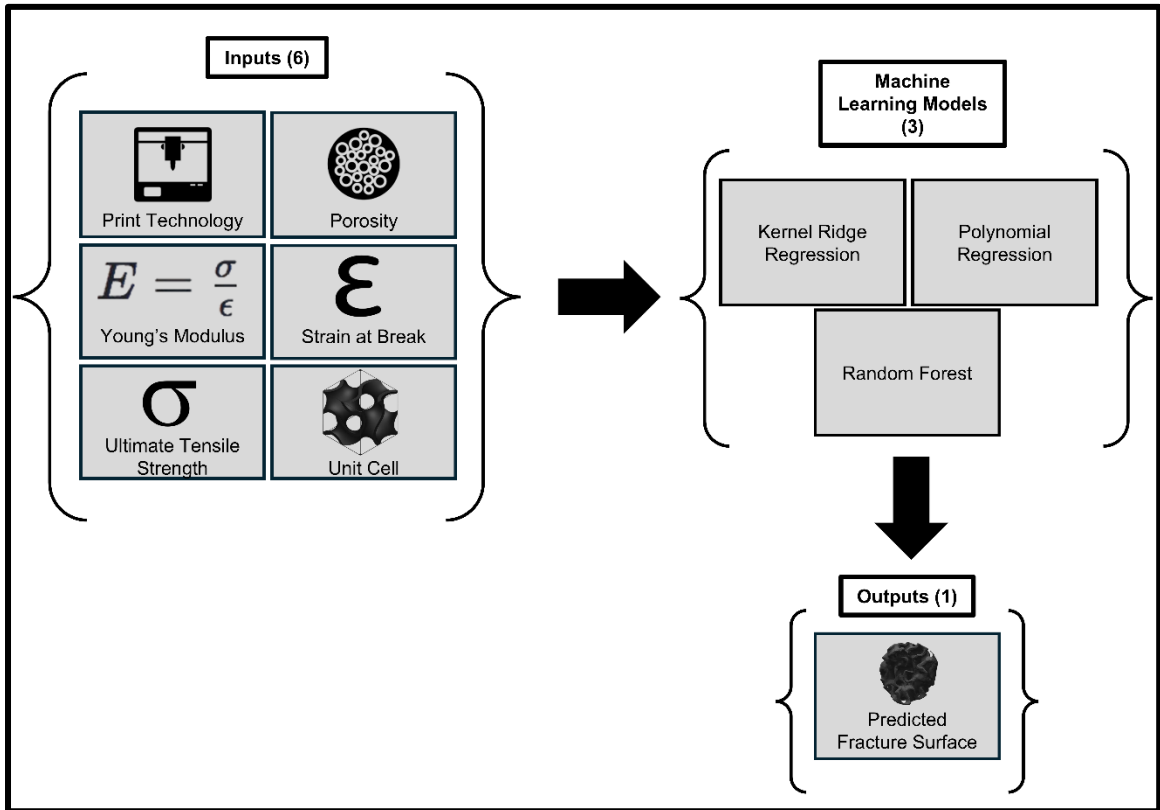


Figure 9: Machine Learning Flowchart.

## 5.5 Evaluating Model Performance

### 5.5.1 Metrics

The primary quantitative metrics used with each algorithm are root mean squared error (RMSE) and the coefficient of determination ( $R^2$ ). Additional metrics such as mean absolute error (MAE), mean absolute percentage error (MAPE), explained variance score, and median absolute error are considered, but the performance of the models can be justified using the former metrics. RMSE is a measure of the square root of the average of the squared differences between predicted and observed data.  $R^2$  is a measure of variance and is described by the ratio of variation in the output that can be predicted to the variation from the inputs.

### **5.5.2 Feature Importance**

Another means for evaluating the performance of the algorithms used is through feature importance. This process shows how much weight each input had in the testing process when trying to predict the fracture surface coefficients. More specifically, the importance of each feature on the outcome of the predicted fracture surface coefficients can be determined by computing the Model Reliance Ratio (MRR). This calculation involves the randomization of the distribution of features and calculates the RMSE of the randomized features with the original RMSE. The feature that shows the largest change in RMSE between the randomized and initial inputs will prove to be the most important as that one will have the largest effect on the model's performance.

### ***5.4 Chapter Summary***

Chapter 5 explains the coding component of the thesis. It begins with the breakdown of the code structure and the way in which the data is processed and prepared for the machine learning segment. It highlights the process of defining the fracture surface of each lattice structure as well as the process of fitting the fourth order surface to the structure and extracting its components as use for the machine learning inputs. In the ML section of this chapter, the inputs and outputs are discussed in addition to the principal components analysis for feature reduction. The chapter closes with the architecture for each of the algorithms being used and the metrics that evaluate the performance of each of the algorithms.

## 6. Results

### 6.1 Porosity

This first section of the Results chapter covers the porosity evaluation. Figure 11 displays the porosity validation results plotted from the weight-based approach explained in the materials and methods chapter. Preceding that is Figure 10, showing the CT scans for each porosity value analyzed. Figure 10 also shows CT data of certain samples that have irregularities because of the printing technologies, and how those deficiencies affect the final porosity of each sample.

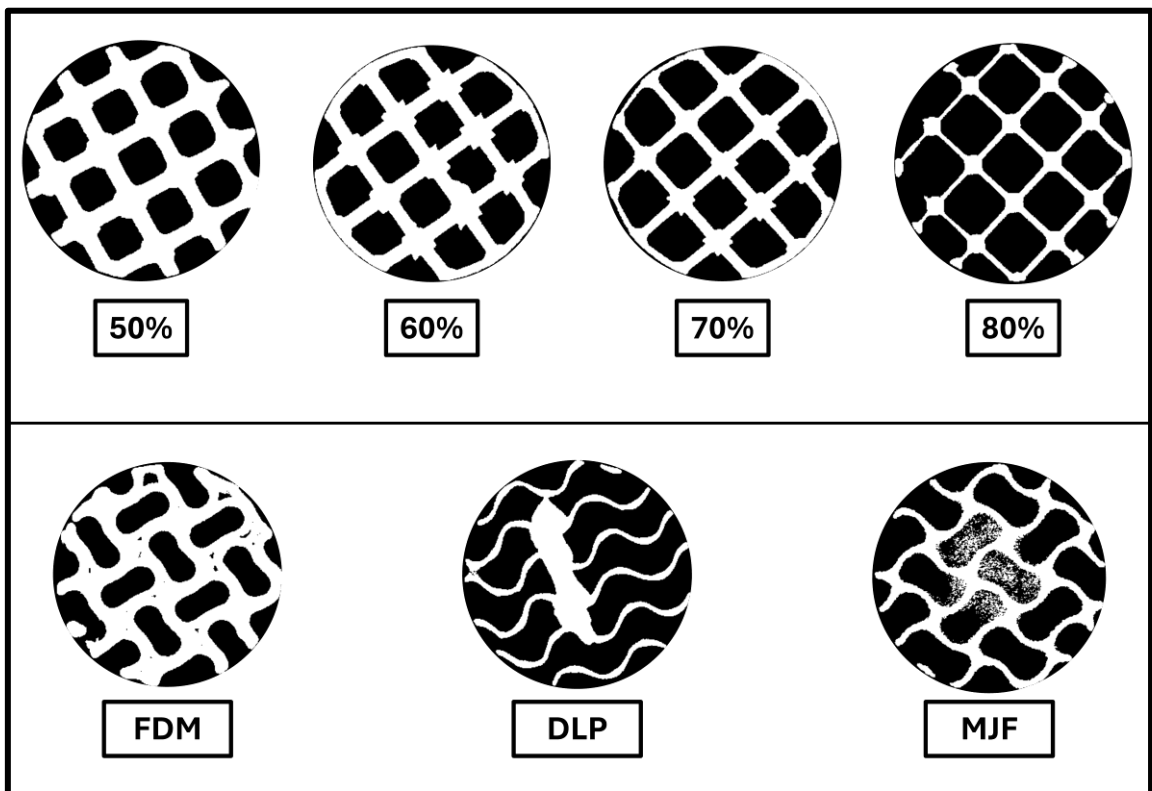


**Figure 10: CT Data Displaying Porosity Values for Octet Lattice Structures and Printing Discrepancies Affecting Porosity.**

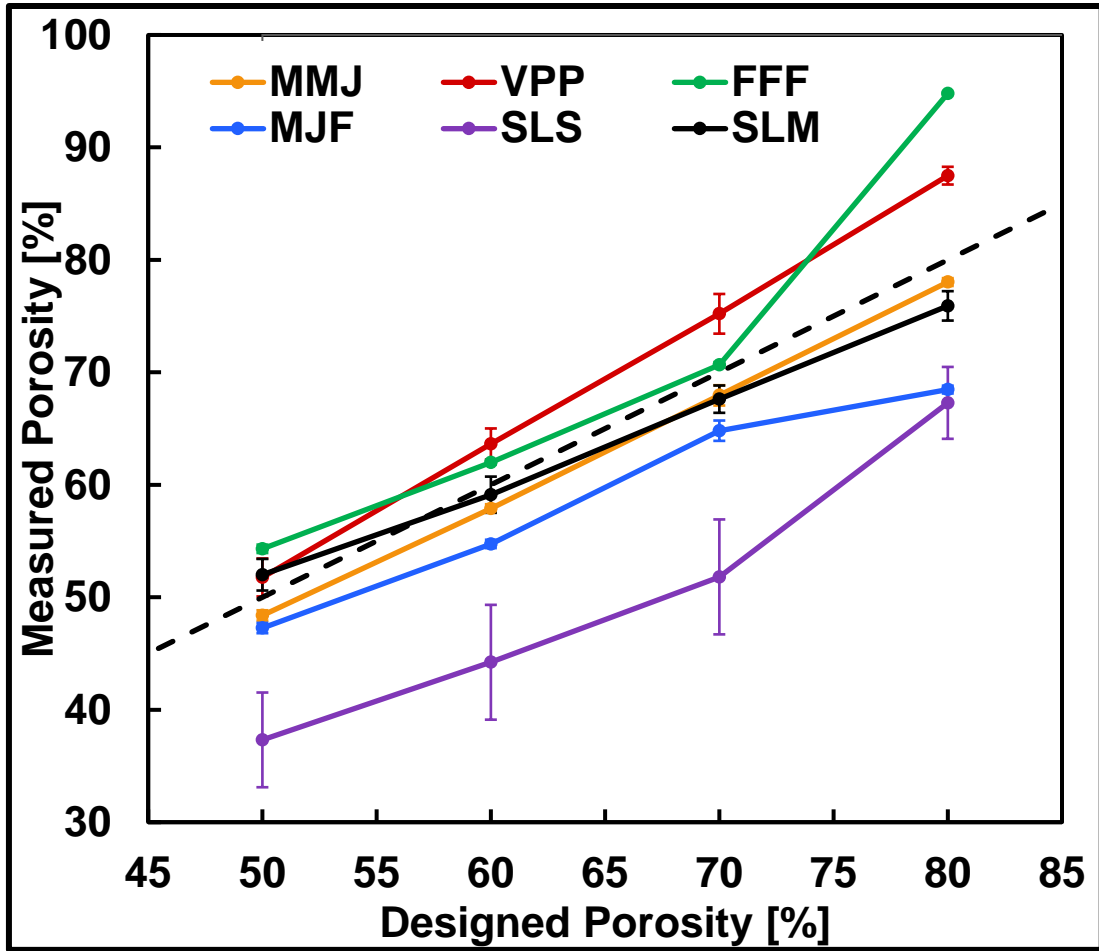


Figure 11: Designed Porosity vs. Experimental Porosity.

[39]

## 6.2 Mechanical Testing

This section covers the mechanical data from the uniaxial tensile test conducted on the lattice and solid structures. Figure 12 below shows the normalized ultimate strength of the lattice structures while Figure 13 shows the relationship between the normalized ultimate strength and the material ultimate strength of the lattices.

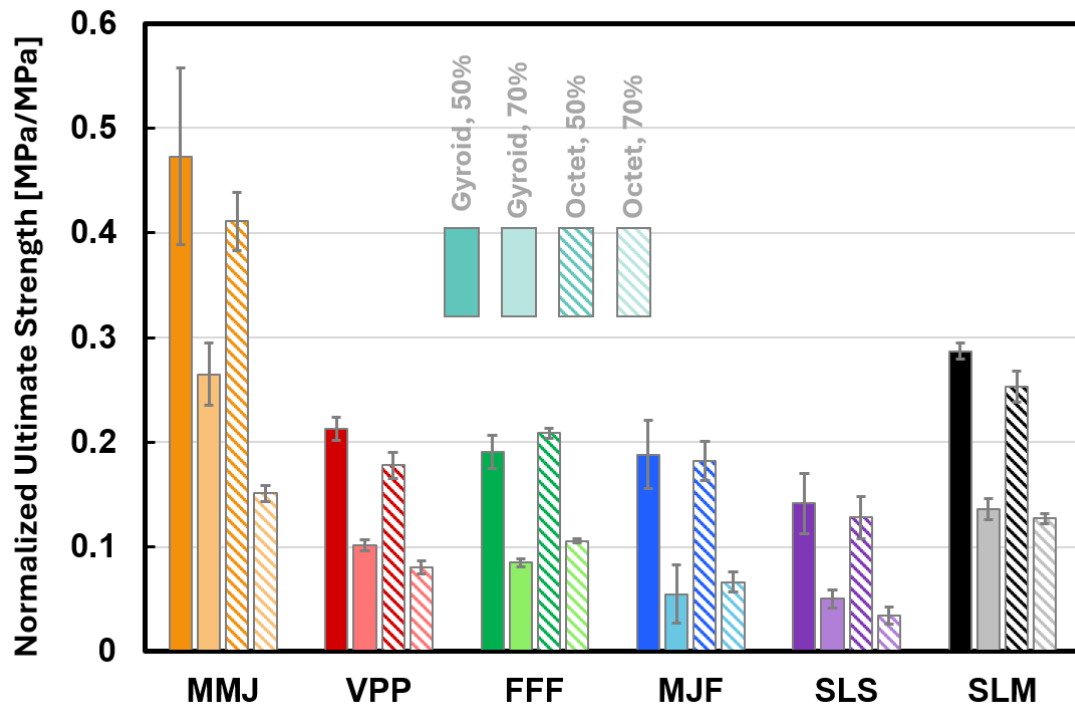


Figure 12: Normalized Lattice Ultimate Strength.  
[39]

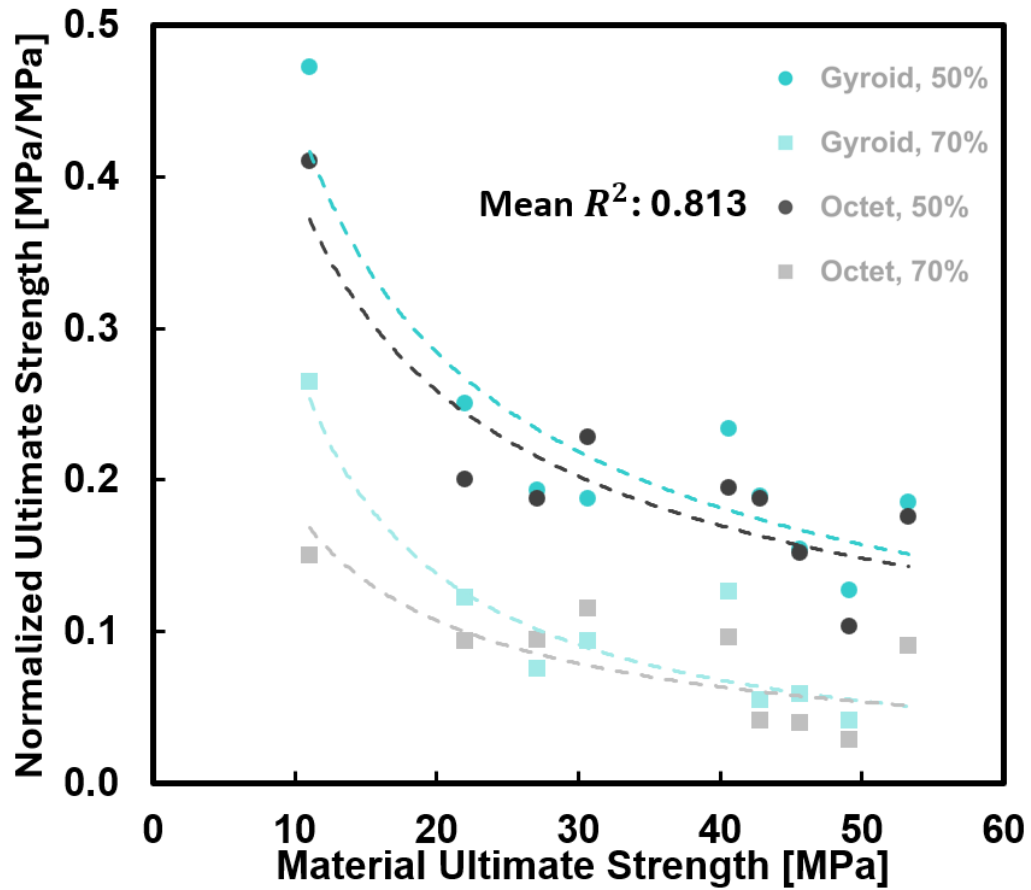
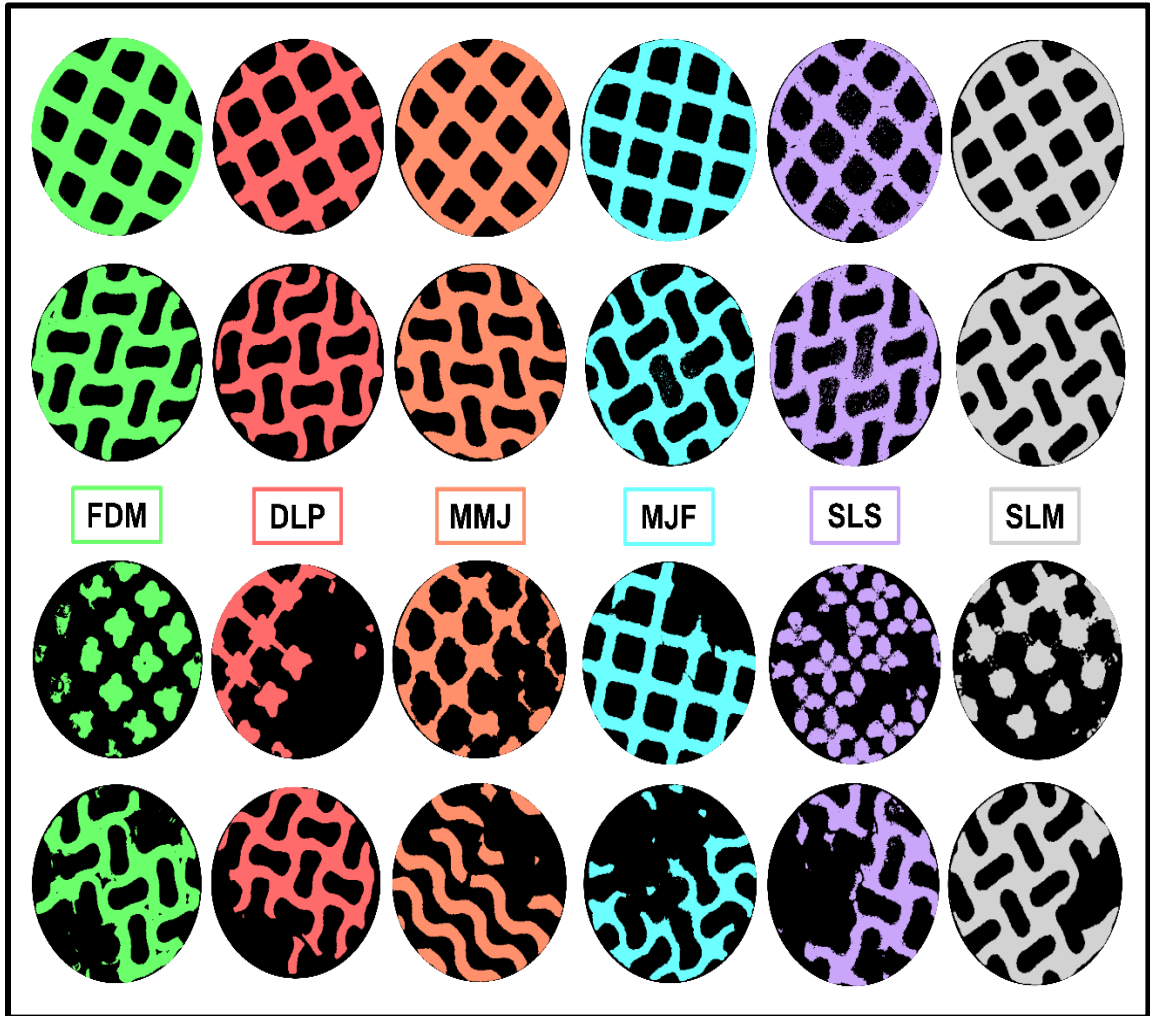


Figure 13: Material Ultimate Strength vs. Normalized Ultimate Strength [39]

### 6.3 Imaging

The imaging results include the CT data and the SEM images that show crack nucleation and propagation in the lattice structures until total failure. CT data provides a broader visual of the entire fracture surface of the lattice through the CT slices, and SEM provides a detailed observation of significant features on the fracture surface. Figure 14 shows slices from the CT scans for each print method and unit cell at 50% porosity before and after the onset of fracture. Figure 15 shows the SEM images taken of each of the print methods and unit cells at 70% porosity with the ETD, T1, and T2 detectors.



**Figure 14: CT Data Showing 50% Porosity Lattice Structures Before and After the Onset of Fracture.**

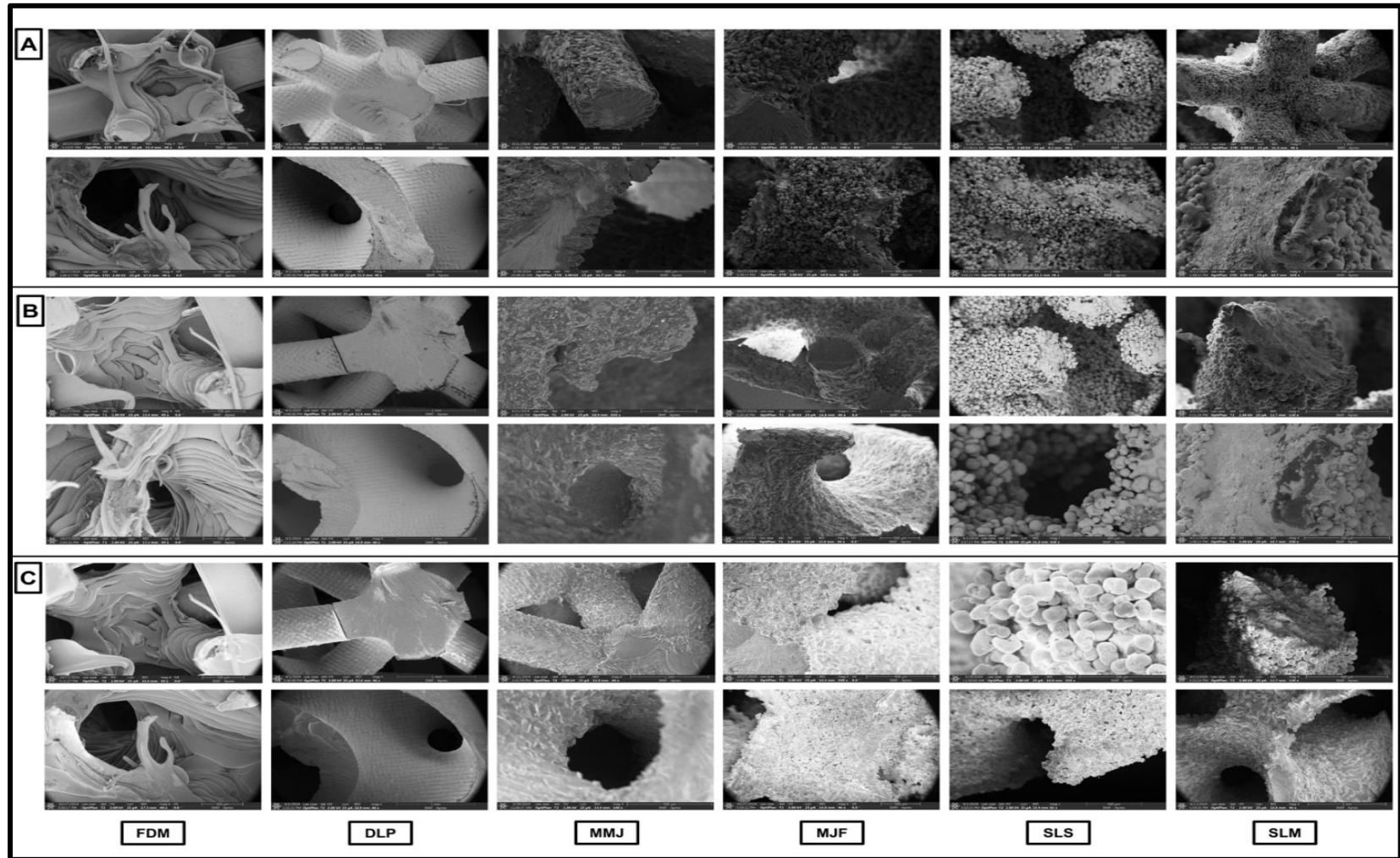


**Figure 15: SEM Images of 70% Porosity Lattice Structures Using Different Detectors.**  
 A) Everhart-Thornley Detector, B) T1 Detector, C) T2 Detector.

## 6.4 Machine Learning

The results of the machine learning aspect of this study comprise the comparison of metrics for each of the models used. Table 2 below shows the model performance in terms of RMSE,  $R^2$ , and MAE.

**Table 2: Machine Learning Model Performance.**

ML Model	Dataset	RMSE	$R^2$	MAE
Kernel Ridge Regression	Training	0.131	0.701	0.0661
	Testing	0.337	-0.715	0.173
Polynomial Regression	Training	0.368	0.105	0.174
	Testing	0.455	-0.00595	0.193
Random Forest	Training	0.149	0.660	0.0801
	Testing	0.333	-0.143	0.160

## 6.5 Chapter Summary

Chapter 6 covers the preliminary results of the study. It considers the porosity validation process and CT data that can potentially support those findings. The second section shows the mechanical testing results in the form of normalized lattice strength and other fundamental properties of the lattice structures. Imaging is shown through the CT and SEM images taken that briefly explain the fracture behavior of the print methods, unit cells, materials, or porosities of the parts. The chapter ends with the performance of the ML models used through the metrics highlighted in 5.5.1.

## **7. Conclusions**

### ***7.1 Discussion***

This chapter highlights all the results shown in Chapter 6 with comments on hypotheses, experimental observations, and conclusions of the entire study. Generally, AM lattice behavior, both mechanical and fracture-based, is difficult to predict. The research does a decent job at collecting the data and representing it in a way that shows the feasibility of combining research in fracture mechanics, additive manufacturing, and machine learning, but there are external factors that play a role in how well these disciplines can be related to one another.

#### **7.1.1 Porosity**

Porosity plays a large role in all phases of the study. Porosity directly affects the ability to print these AM lattices because it primarily controls the minimum feature size. It affects testing because strength tends to be proportional to the decrease in porosity, meaning that a structure that is 50% porous should be stronger and take longer to reach failure compared to a structure with 80% porosity. Figure 11 shows that many of the structures tend to be under porous, while FDM and DLP tend to be over porous printing methods. The most accurate printing method in terms of porosity comes from the MMJ prints with VJC.

Additionally, the bottom section of Figure 10 highlights the printing imperfections that affect porosity. In FDM, the anisotropy and constraints on the nozzle size and movement present itself in the missing infill. The infill density is 100% such that these parts are completely solid where material is being extruded, but the complexity of these lattice structures shows up immensely in this instance. In DLP, there is trapped resin that ideally would be removed from the isopropanol wash in the post-processing steps, but because of how small these parts are, it is still within reason for resin to get stuck inside and then cure permanently once the rest of the structure undergoes curing. In the powder-based methods like MJF, porosity is affected by the

accumulation of powder particles inside the pores. Particles that do not fully fuse with one another during the printing process become stuck on the inside of these tight crevices and cannot be removed until after it is exposed through mechanical testing or with the use of pressurized air to blow the excess powder out.

### **7.1.2 Mechanical Performance**

Figure 12 shows that the normalized lattice strength relative to the solid structure is highest for the MMJ print method. This went against an initial hypothesis because of how quickly these parts broke and to the degree in which they completely shattered. This is due to poor tensile properties and brittleness in the solid samples, which in turn creates a higher perceived normalized strength. The remaining normalized lattice strength values are in decreasing order from SLM, DLP, FDM, MJF with SLS having the lowest normalized ultimate strength. This drastic change in normalized ultimate strength between SLM and SLS is likely due to the higher surface roughness in SLS and the better cohesion within the structures due to enhanced melt pool formation in SLM. [39]

In terms of normalized strain at failure, there is a similar trend where it is observed that MMJ has the highest normalized strain at break. This continues to FDM, DLP, MJF, SLM, and SLS, respectively. Holistically, MMJ lattices have the highest normalized mechanical values while SLS structures have the lowest. Again, this is due to deficient performance by the normalizer in MMJ. Across both the normalized lattice strength and normalized strain at break, gyroid structures perform better in terms of normalized strengths than octet unit cells. [39]

Lastly, it can be observed in Figure 13 that the ultimate strength of the polymeric lattices can be described by a power function using the material's ultimate strength as well. This suggests that mechanical performance is directly related to material characteristics and that performance may be scalable and predictable. [39]

### 7.1.3 Fracture Mechanics

As introduced at the beginning of the paper, the fracture behavior of lattice structures is difficult to characterize and predict because of the variability in how the samples break. The anisotropic nature of AM, coupled with the complexity and periodicity of the structure, results in fracture mechanisms that are not easily described by traditional fracture models. This was evident primarily in FDM and certain MJF prints, and especially in structures designed with the gyroid unit cell.

Many of the materials displayed standard fracture, breaking in a uniform position and manner for each sample, resulting in an expected sharp drop after moving through the elastic, strain hardening, and necking regions. This was not the case in many FDM and MJF prints as the interconnectivity and fusion of the layers in these print methods showed elastic-plastic properties. These structures would display a gradual decline at the end of the necking region and the fracture segments of the lattice would remain connected to one another by single strands of print material. This phenomenon was evident in structures using the gyroid as opposed to the octet-truss because of its sinusoidal nature. The octet unit cell has struts that can be broken with ease and consistency that would result in a uniform fracture surface, whereas the gyroid relies on the surface definition.

Another interesting observation was the way in which the structures broke. Samples fabricated using MMJ fractured with significant ease and shattered. The testing speed is slow enough such that parts should be able to fit back together after fracture like a puzzle piece. This was not the case for MMJ, as the parts would not break in just one area but would split the part into multiple pieces. Fracture sometimes occurred in the solid tabs as well that were just meant to hold the structure inside the grips of the testing machine. These same observations were made for DLP, but on a lesser scale, likely because they are both resin-based printing methods, but DLP resins are more viscous. LPBF structures were also interesting at the notion of total failure

because trapped powder inside the cells of the lattice would often be ejected and would accumulate at the exposed surface.

#### **7.1.4 Machine Learning**

The ML component of the research provided interesting insights as to how well the data can be predicted and how much variance can be explained through models desiring a complex output of 15 coefficient values (or 10 considering feature reduction). Based on the data presented in Table 2, the superior performing model based on RMSE of the testing dataset was the Random Forest, followed by Kernel Ridge and Polynomial Regressions, respectively. All the models performed poorly at capturing the variability in the study, as denoted by negative  $R^2$  values. The least negative  $R^2$  value comes from the Polynomial Regression, which reasonably correlates with the connection I hypothesized when considering which models to use. Generally, the results suggest that these current machine learning models cannot accurately characterize the fracture surfaces of these lattice structures. This is largely due to the complexity of the structures but could also be affected by correlation instability from having structures and outputs that use the same or similar input parameters. This points to why the qualitative analysis of the structures through the imaging methods tends to provide more digestible information about these exposed surfaces. There are tradeoffs in choosing the values for hyperparameters in each of the algorithms that might better explain variability while increasing the error. Ultimately, this study focused on the RMSE as its primary evaluation metric, which proved a random forest predicts the fracture surface coefficient with decent accuracy. The preliminary MRR assessment for feature importance also suggested that porosity was the most important factor in successfully predicting the coefficients of the fracture surfaces.

Additionally, the general fit of the fourth order surface to the broken lattice structure is fairly accurate to the naked eye. There are some discrepancies that arise from edge effects and the lack of bounding to the exact dimensions of the lattice structure, but nonetheless, the surface

explains the fracture of each configuration well. This could likely be improved with a tighter grid that generates more points in the point cloud, but since the more significant coefficients of the total 15 start to plateau and reach asymptotic values, this is not necessary as it increases the computational load required to determine the plane.

## ***7.2 Future Work***

Future work for this study occurs primarily through the machine learning components by trying to make models perform better but can be extended to other aspects. One potential for future work is expanding the data being collected. One way this could be done is through the inclusion of more materials and/or printing technologies. Generally, this is a very expansive range of variables when considering unit cell, porosity, material, and print method. A better way to influence the amount of data collected is because this study focuses on purely uniaxial tension; however, data is in the process of being collected for these same samples being tested in uniaxial compression and multiaxial torsion. This provides more information about the mechanical properties of each lattice structure configuration, but also expands the way in which fracture occurs since the loading mode is different.

Continuing with data collection, the study is a bit skewed in the sense that not all the structures break under tension. Some of the structures, dependent on their inputs, are strong enough to withstand the entire displacement in the duration of the tensile test. Since these parts do not result in an exposed fracture surface, these cannot be imaged, and therefore affect the number of samples in the study. This same problem occurs even at earlier steps where certain parts suffer from limitations on minimum feature size and cannot be fabricated. Determining a way to account for any of these structures would be interesting if possible.

It would also be beneficial to work to capture more variability from the way the fracture occurs for different samples. As said in 7.1.3, FDM showed a significant amount of variability in the way the structures broke under tensile loading. Between the end of the mechanical tests, and

the reconstruction of the samples through ImageJ, a lot of variability is lost as noise in the software. This results in multiple structures appearing to have primarily flat macroscale fracture surfaces because less of that variability is being retained. This could be altered by better post-processing, limitations on the mesh reduction process if this significantly affects the resolution of the samples, and potentially increasing the testing speed to result in a more abrupt fracture mechanism.

As mentioned, the machine learning component of the study is the primary area of future work. An ideal discovery out of these initial results is to be able to run the study in reverse. More specifically, one should be able to take the fracture information from the superior performing ML models, choose the desired fracture surface and have the model work backwards to output the combination of print method, material, unit cell, and porosity. Fabricate and test that structure under the loading condition specified, then work back through the ML model in its original form to analyze if the STL file generated from the reverse-engineered fracture surface matches the fracture surface coefficients that were started with within a certain tolerance of a given evaluation metric.

ML can also be improved with potential future work by making the model more complex. More evaluation into deep learning and potentially convolutional neural networks or an image-based model like AlexNet could be beneficial to the understanding and predictability of the lattice structure fracture behavior. This could also lead to a more in-depth fracture analysis. This could include more dedicated research on crack nucleation and propagation, the inclusion of fatigue testing, and finite element analysis for the variable loading conditions.

## References

1. Ali, M., Sajjad, U., Hussain, I., Abbas, N., Ali, H. M., Yan, W. M., & Wang, C. C. (2022). On the assessment of the mechanical properties of additively manufactured lattice structures. *Engineering Analysis with Boundary Elements*, *142*, 93–116. <https://doi.org/10.1016/J.ENGANABOUND.2022.05.019>
2. Al-Jassir, F. F., Fouad, H., & Alothman, O. Y. (2013). In vitro assessment of Function Graded (FG) artificial Hip joint stem in terms of bone/cement stresses: 3D Finite Element (FE) study. *BioMedical Engineering Online*, *12*(1), 1–17. <https://doi.org/10.1186/1475-925X-12-5/FIGURES/15>
3. Al-Ketan, O., Rowshan, R., & Abu Al-Rub, R. K. (2018). Topology-mechanical property relationship of 3D printed strut, skeletal, and sheet based periodic metallic cellular materials. *Additive Manufacturing*, *19*, 167–183. <https://doi.org/10.1016/j.addma.2017.12.006>
4. Arabnejad Khanoki, S., & Pasini, D. (2012). Multiscale design and multiobjective optimization of orthopedic hip implants with functionally graded cellular material. *Journal of Biomechanical Engineering*, *134*(3). <https://doi.org/10.1115/1.4006115/465218>
5. Arabnejad, S., Johnston, B., Tanzer, M., & Pasini, D. (2017). Fully porous 3D printed titanium femoral stem to reduce stress-shielding following total hip arthroplasty. *Journal of Orthopaedic Research*, *35*(8), 1774–1783. <https://doi.org/10.1002/JOR.23445>
6. Brown, P. J. (2016). *SELECTIVE LASER SINTERING (SLS) RAPID PROTOTYPING TECHNOLOGY: A REVIEW OF MEDICAL APPLICATIONS*. <https://www.researchgate.net/publication/305851453>
7. Cai, C., Tey, W. S., Chen, J., Zhu, W., Liu, X., Liu, T., Zhao, L., & Zhou, K. (2021). Comparative study on 3D printing of polyamide 12 by selective laser sintering and multi jet fusion. *Journal of Materials Processing Technology*, *288*, 116882. <https://doi.org/10.1016/J.JMATPROTEC.2020.116882>
8. Cantaboni, F., Battini, D., Hauber, K. Z., Ginestra, P. S., Tocci, M., Avanzini, A., Ceretti, E., & Pola, A. (123 C.E.). Mechanical and microstructural characterization of Ti6Al4V lattice structures with and without solid shell manufactured via electron beam powder bed fusion. *The International Journal of Advanced Manufacturing Technology*, *131*, 1289–1301. <https://doi.org/10.1007/s00170-024-13137-2>
9. Chaudhary, R., Fabbri, P., Leoni, E., Mazzanti, F., Akbari, R., & Antonini, C. (2022). Additive manufacturing by digital light processing: a review. *Progress in Additive Manufacturing* *2022* 8:2, *8*(2), 331–351. <https://doi.org/10.1007/S40964-022-00336-0>
10. Cui, X., Xue, Z., Pei, Y., & Fang, D. (2011). Preliminary study on ductile fracture of imperfect lattice materials. *International Journal of Solids and Structures*, *48*(25–26), 3453–3461. <https://doi.org/10.1016/J.IJSOLSTR.2011.08.013>

11. Daneshdoost, N., & Gall, K. (2023). Mechanical Behavior of Multi-material Jetting Polymeric Composites Designed at the Voxel Scale: Expanding Beyond the Capabilities of Preset Material Blends. *SSRN Electronic Journal*.  
<https://doi.org/10.2139/SSRN.4687602>
12. Dohan Ehrenfest, D. M., Coelho, P. G., Kang, B. S., Sul, Y. T., & Albrektsson, T. (2010). Classification of osseointegrated implant surfaces: Materials, chemistry and topography. *Trends in Biotechnology*, 28(4), 198–206.  
<https://doi.org/10.1016/J.TIBTECH.2009.12.003/ASSET/63BCAF-8B64-45CC-8C88-8F2B1B165E1D/MAIN.ASSETS/GR2.SML>
13. Dudek, P. (2013). FDM 3D printing technology in manufacturing composite elements. *Archives of Metallurgy and Materials*, 58(Vol. 58, iss. 4), 1415--1418.  
<https://doi.org/10.2478/AMM-2013-0186>
14. Gongora, A. E., Friedman, C., Newton, D. K., Yee, T. D., Doorenbos, Z., Giera, B., Duoss, E. B., Y-J Han, T., Sullivan, K., & Rodriguez, J. N. (123 C.E.). Accelerating the design of lattice structures using machine learning. *Scientific Reports* /, 14, 13703.  
<https://doi.org/10.1038/s41598-024-63204-7>
15. Gu, H., Shterenlikht, A., & Pavier, M. (2019). *Brittle fracture of three-dimensional lattice structure*. <https://doi.org/10.1016/j.engfracmech.2019.106598>
16. Hasanov, S., Alkunte, S., Rajeshirke, M., Gupta, A., Huseynov, O., Fidan, I., Alifui-Segbaya, F., & Rennie, A. (2021). Review on Additive Manufacturing of Multi-Material Parts: Progress and Challenges. *Journal of Manufacturing and Materials Processing* 2022, Vol. 6, Page 4, 6(1), 4. <https://doi.org/10.3390/JMMP6010004>
17. Heimbrook, A., Kelly, C., & Gall, K. (2022a). Effects of 3D printed surface topography and normal force on implant expulsion. *Journal of the Mechanical Behavior of Biomedical Materials*, 130, 105208. <https://doi.org/10.1016/J.JMBBM.2022.105208>
18. Heimbrook, A., Kelly, C., & Gall, K. (2022b). Interface contact behavior of 3D printed porous surfaces. *Journal of Materials Research and Technology*, 21, 4115–4126.  
<https://doi.org/10.1016/J.JMRT.2022.10.104>
19. Hooshmand, M. J., Sakib-Uz-Zaman, C., & Khondoker, M. A. H. (2023). Machine Learning Algorithms for Predicting Mechanical Stiffness of Lattice Structure-Based Polymer Foam. *Materials*, 16(22). <https://doi.org/10.3390/ma16227173>
20. Kelly, C. N., Evans, N. T., Irvin, C. W., Chapman, S. C., Gall, K., & Safranski, D. L. (2019). The effect of surface topography and porosity on the tensile fatigue of 3D printed Ti-6Al-4V fabricated by selective laser melting. *Materials Science and Engineering: C*, 98, 726–736. <https://doi.org/10.1016/J.MSEC.2019.01.024>
21. Kelly, C. N., Francovich, J., Julmi, S., Safranski, D., Guldborg, R. E., Maier, H. J., & Gall, K. (2019). Fatigue behavior of As-built selective laser melted titanium scaffolds with sheet-based gyroid microarchitecture for bone tissue engineering. *Acta Biomaterialia*, 94, 610–626. <https://doi.org/10.1016/J.ACTBIO.2019.05.046>

22. Kelly, C. N., Miller, A. T., Hollister, S. J., Guldborg, R. E., & Gall, K. (2018). Design and Structure–Function Characterization of 3D Printed Synthetic Porous Biomaterials for Tissue Engineering. *Advanced Healthcare Materials*, 7(7), 1701095. <https://doi.org/10.1002/adhm.201701095>
23. Khan, N., & Riccio, A. (2024). A systematic review of design for additive manufacturing of aerospace lattice structures: Current trends and future directions. *Progress in Aerospace Sciences*, 149, 101021. <https://doi.org/10.1016/J.PAEROSCI.2024.101021>
24. Kristiawan, R. B., Imaduddin, F., Ariawan, D., Ubaidillah, & Arifin, Z. (2021). A review on the fused deposition modeling (FDM) 3D printing: Filament processing, materials, and printing parameters. *Open Engineering*, 11(1), 639–649. [https://doi.org/10.1515/ENG-2021-0063/ASSET/GRAPHIC/J\\_ENG-2021-0063\\_FIG\\_003.JPG](https://doi.org/10.1515/ENG-2021-0063/ASSET/GRAPHIC/J_ENG-2021-0063_FIG_003.JPG)
25. Mahmoud, D., & Elbestawi, M. A. (2017). Lattice Structures and Functionally Graded Materials Applications in Additive Manufacturing of Orthopedic Implants: A Review. *Journal of Manufacturing and Materials Processing 2017*, Vol. 1, Page 13, 1(2), 13. <https://doi.org/10.3390/JMMP1020013>
26. Mahmoudi, M., Ghannadpour, S. A. M., & Nedjad, K. H. (2024). Functionally graded multi-morphology lattice structures as an optimized sandwich core via digital light processing additive manufacturing. *Materials & Design*, 238, 112710. <https://doi.org/10.1016/J.MATDES.2024.112710>
27. Nabavi-Kivi, A., Ayatollahi, M. R., Schmauder, S., & Khosravani, M. R. (2023). Fracture Analysis of a 3D-Printed ABS Specimen: Effects of Raster Angle and Layer Orientation. *Physical Mesomechanics*, 26(1), 19–32. <https://doi.org/10.1134/S1029959923010034/FIGURES/16>
28. Olakanmi, E. O., Cochrane, R. F., & Dalgarno, K. W. (2015). A review on selective laser sintering/melting (SLS/SLM) of aluminium alloy powders: Processing, microstructure, and properties. *Progress in Materials Science*, 74, 401–477. <https://doi.org/10.1016/J.PMATSCI.2015.03.002>
29. Peloquin, J., Kirillova, A., Mathey, E., Rudin, C., Brinson, L. C., & Gall, K. (2023). Tensile performance data of 3D printed photopolymer gyroid lattices. *Data in Brief*, 49, 109396. <https://doi.org/10.1016/J.DIB.2023.109396>
30. Peloquin, J., Kirillova, A., Rudin, C., Brinson, L. C., & Gall, K. (2023). Prediction of tensile performance for 3D printed photopolymer gyroid lattices using structural porosity, base material properties, and machine learning. *Materials & Design*, 232, 112126. <https://doi.org/10.1016/J.MATDES.2023.112126>
31. Šafka, J., Ackermann, M., Vele, F., Macháček, J., & Henyš, P. (2021). Mechanical Properties of Polypropylene: Additive Manufacturing by Multi Jet Fusion Technology. *Materials 2021*, Vol. 14, Page 2165, 14(9), 2165. <https://doi.org/10.3390/MA14092165>
32. Santoliquido, O., Colombo, P., & Ortona, A. (2019). Additive Manufacturing of ceramic components by Digital Light Processing: A comparison between the “bottom-up” and the

“top-down” approaches. *Journal of the European Ceramic Society*, 39(6), 2140–2148. <https://doi.org/10.1016/J.JEURCERAMSOC.2019.01.044>

33. Schneider, J., & Kumar, S. (2023). Comparative performance evaluation of microarchitected lattices processed via SLS, MJ, and DLP 3D printing methods: Experimental investigation and modelling. *Journal of Materials Research and Technology*, 26, 7182–7198. <https://doi.org/10.1016/j.jmrt.2023.09.061>
34. Spadoni, A., & Ruzzene, M. (2007). Numerical and experimental analysis of the static compliance of chiral truss-core airfoils. *Journal of Mechanics of Materials and Structures*, 2(5), 965–981. <https://doi.org/10.2140/JOMMS.2007.2.965>
35. Timercan, A., Terriault, P., & Brailovski, V. (2023). Axial tension/compression and torsional loading of diamond and gyroid lattice structures for biomedical implants: Simulation and experiment. *Materials and Design*, 225. <https://doi.org/10.1016/j.matdes.2022.111585>
36. Wang, C., Tan, X. P., Tor, S. B., & Lim, C. S. (2020). Machine learning in additive manufacturing: State-of-the-art and perspectives. *Additive Manufacturing*, 36, 101538. <https://doi.org/10.1016/J.ADDMA.2020.101538>
37. Wu, C., Wan, B., Entezari, A., Fang, J., Xu, Y., & Li, Q. (2024). Machine learning-based design for additive manufacturing in biomedical engineering. *International Journal of Mechanical Sciences*, 266, 108828. <https://doi.org/10.1016/J.IJMECSCI.2023.108828>
38. Yap, C. Y., Chua, C. K., Dong, Z. L., Liu, Z. H., Zhang, D. Q., Loh, L. E., & Sing, S. L. (2015). Review of selective laser melting: Materials and applications. *Applied Physics Reviews*, 2(4). <https://doi.org/10.1063/1.4935926/123739>
39. Daneshdoost, N., Peloquin, J., Heimbrook, A., Sampson, F., Lennon, R., & Gall, K. (2024, October 28). *Effect of additive manufacturing fabrication method on the multimodal mechanical properties of porous architectures* [Poster presentation]. ICAM 2024 Conference, Atlanta, GA.